Université de Montréal

CALMODULIN/KCa3.1 CHANNEL INTERACTIONS AS DETERMINANT TO THE KCa3.1 Ca^{2+} DEPENDENT GATING: THEORETICAL AND EXPERIMENTAL ANALYSES

par
Patricia Morales Espinosa

Département de Physique
Faculté des Études Supérieures

Mémoire présenté à la Faculté des études supérieures
en vue de l'obtention du grade de Maître ès Sciences (M. Sc.) en physique
option Biophysique et Physiologie Moléculaire

Décembre 2010

Université de Montréal
Faculté des études supérieures

Ce mémoire intitulé:Calmodulin/KCa3.1 channel interactions as determinant to the KCa3.1 Ca^{2+} dependent gating: Theoretical and experimental analyses

présenté par:
Patricia Morales Espinosa

a été évalué par un jury composé des personnes suivantes:

Jean-Yves Lapointe
président-rapporteur
Rémy Sauvé
directeur de recherche
Rikard Blunck
membre du jury

Résumé

Differentes études ont montré que la sensibilité au Ca^{2+}du canal K_{Ca}3.1, un canal potassique indépendant du voltage, était conférée par la protéine calmoduline (CaM) liée de façon constitutive au canal. Cette liaison impliquerait la région C-lobe de la CaM et un domaine de K_{Ca}3.1 directement relié au segment transmembranaire S6 du canal. La CaM pourrait également se lier au canal de façon Ca^{2+} dépendante via une interaction entre un domaine de K_{Ca}3.1 du C-terminal (CaMBD2) et la région N-lobe de la CaM. Une étude fut entreprise afin de déterminer la nature des résidus responsables de la liaison entre le domaine CaMBD2 deK_{Ca}3.1 et la région N-lobe de la CaM et leur rôle dans le processus d'ouverture du canal par le Ca^{2+}.

Une structure 3D du complexe KCa3.1/CaM a d'abord été générée par modélisation par homologie avec le logiciel MODELLER en utilisant comme référence la structure cristalline du complexe SK_{Ca}2.2/CaM (PDB: 1G4Y). Le modèle ainsi obtenu de K_{Ca}3.1 plus CaM prévoit que le segment L361-S372 dans KCa3.1 devrait être responsable de la liaison dépendante du Ca^{2+} du canal avec la région N-lobe de la CaM via les résidus L361 et Q364 de K_{Ca}3.1 et E45, E47 et D50 de la CaM. Pour tester ce modèle, les résidus dans le segment L361-S372 ont été mutés en Cys et l'action du $MTSET^+$ (chargé positivement) et MTSACE (neutre) a été mesurée sur l'activité du canal.

Des enregistrements en *patch clamp* en configuration "*inside-out*" ont montré que la liaison du réactif chargé $MTSET^+$ au le mutant Q364C entraîne une forte

augmentation du courant, un effet non observé avec le MTSACE. De plus les mutations E45A et E47A dans la CaM, ont empêché l'augmentation du courant initié par $MTSET^+$ sur le mutant Q364C. Une analyse en canal unitaire a confirmé que la liaison $MTSET^+$ à Q364C cause une augmentation de la probabilité d'ouverture de $K_{Ca}3.1$ par une déstabilisation de l'état fermé du canal.

Nous concluons que nos résultats sont compatibles avec la formation de liaisons ioniques entre les complexes chargés positivement Cys-$MTSET^+$ à la position 364 de $K_{Ca}3.1$ et les résidus chargés négativement E45 et E47 dans la CaM. Ces données confirment qu'une stabilisation électrostatique des interactions CaM/-KCa3.1 peut conduire à une augmentation de la probabilité d'ouverture du canal en conditions de concentrations saturantes de Ca^{2+}.

Mots clés: Modelisation par Homologie, KCa3.1, electrophysiologie, MTS reagents, Calmodulin(CaM).

Abstract

The Ca^{2+}sensitivity of the voltage-insensitive calcium activated potassium channel of intermediate conductance K_{Ca}3.1 is conferred by calmodulin (CaM) constitutively bound to the membrane-proximal region of the channel intracellular C - terminus. A study was performed to investigate the nature of the residues involved in the CaM/K_{Ca}3.1 interactions and determine how these interactions could modulate the channel gating properties.

A 3D-structure of the KCa3.1/CaM complex was first generated by homology modeling with MODELLER using as template the crystal structure of SK_{Ca}2.2/CaM complex (PDB: 1G4Y). The resulting structural model of K_{Ca}3.1 plus CaM predicts that the segment L361-S372 in KCa3.1 should be responsible for the Ca^{2+}-dependent binding of the channel to the CaM-N lobe, with residues L361 and Q364 facing residues E45, E47 and D50 of CaM. To test this model residues in L361-S372 segment were substituted by Cys and the action of $MTSET^{+}$(positive charged) and MTSACE (neutral charged) measured on channel activity.

Inside-out patch clamp recordings showed that the binding of the charged $MTSET^{+}$ reagent to the Q364C mutant resulted in a strong current increase, an effect not seen with the neutral MTSACE. The mutations E45A and E47A in CaM prevented the current increase initiated by $MTSET^{+}$ on the Q364C mutant. A single channel analysis confirmed that the binding of $MTSET^{+}$ to Q364C caused an increase in the channel open probability by a destabilization of the channel closed

state.

Altogether, our results are compatible with the formation of ionic bonds between the positively charged Cys-MTSET$^+$ complex at position 364 in K_{Ca}3.1 and the negatively charged E45 and E47 residues in CaM, and confirm that an electrostatic stabilization of the CaM/KCa3.1 interactions can lead to an increase in the channel open probability at saturating Ca^{2+}.

Keywords: Homology Modeling, potassium channel, KCa3.1, Electrophysiology, MTS reagents, Calmodulin(CaM).

LIST OF ABBREVIATIONS

CaM	Calmodulin
CaMBD	Calmodulin binding domain
CaMBD1	Calmodulin binding first domain
CaMBD2	Calmodulin binding second domain
Cys	Cystein
CyPPA	Ciclohexyl-[2-(3,5-dimethypyrazol-1-yl)-6-methyl-pyramidin -4-yl]-amine
EBIO	1-ethyl-2-benzimidazolinone
MOF	MODELLER Objetive Function
MTS	Methane thiosulfonate
$MTSEA^+$	[2-Amino-ethyl] Methanethiosulfonate hydrobromide
$MTSES^-$	Sodium (2-Sulfonatoethyl) Methanethiosulfonate
$MTSET^+$	[2-(trimethylammonium)ethyl] Methanethiosulfonate bromide
$MTSPtrEA^+$	[3-(Triethylammonium)propyl] Methanthiosulfonate bromide
NDPK-B	Nucleoside Diphosphate Kinase B
P_o	Open probability
$P_{o_{max}}$	Maximal open probability
RMSD	Root Mean Square Distance
SCAM	Substituted-Cystein Accessibility Method

Contents

List of Tables

List of Figures

For

my mother, Neffer Maria Espinosa

and

my father, Augusto Cesar Morales

Acknowledgments

I wish to thank professor Rémy Sauvé for his kind support and confidence he deposited on me since the beginning of my Master studies, thanks to him, I feel that my learning of biophysics was fulfilled beyond my expectancies. I have to thank the members of our laboratory staff: Line Garneau et Hélén Klein, by their support during my studies and research in the laboratory and their patience in my (ongoing) learning process of two new languages. Other members of the *Groupe des études des Protéines Membranaires* (GEPROM) deserve a kind acknowledgement as well: Julie Vernier, Bernadette Wallendorf and Michel Brunette who collaborated to support and teach me all those tricky, but essential skills of the laboratory work that only are learned with practice. I thank the Ministère de l'éducation de Québec, for its fellowship that facilitated my studies. A big acknowledgment to the support of my dear friend Zarah Batulan (*La Comadre*), who helped me a lot correcting my english in the text.

To all my family, specially my husband Arturo whose love and support have been for me a lighthouse all these months.

Chapter 1

Introduction

1.1 Molecular transport mechanisms through biological membranes

Biological membranes are one of the most important components of the living cells. Their main function is to establish a *selective permeable barrier* between different internal and external enviroments both in cells and organelles, allowing cells to maintain a homeostatic state by the control of movement of charged and neutral molecules across the membrane, processes named transport mechanisms.

Lipids in membranes constitute an effective energy barrier to the passage of polar molecules or ions. Only gases such as NO, CO_2, O_2 and lipid-soluble molecules (ether, chloroform, steroids) cross the membrane by free diffusion. From a thermodynamic perspective, if an ion is transfered from water to a lipid medium, we can estimate the solvation free energy (ΔG_{sol}) necessary for that process using a generalized Born model (Hodgkin and Keynes, 1920) such that:

$$\Delta G_{\text{sol}} = -\frac{q^2}{2R_{\text{ion}}}\left(\frac{1}{\epsilon_w} - \frac{1}{\epsilon_l}\right) \tag{1.1}$$

where ϵ_l is the lipid dielectric constant, ϵ_w the water dielectric constant, q the ion electrical charge and R the ionic radius. For $\epsilon_l = 2$,$\epsilon_w = 80$ and R=1.33Å for a potassium ion (K^+), ΔG_{sol} value is 100kcal/mol, a value too high to allow the diffusion of charged molecules or ions across the membrane. This can, however, be achieved through integral membrane proteins with *selective* pores that serve as media of low resistance (ϵ_p of a protein is 78) for the passage of ions and/or charged molecules.

Transmembrane transport can be carried out through two distinct processes referred to as *Facilitated diffusion* and *Active transport*. The first does not use metabolic energy to catalyze the diffusion of the molecules across membrane proteins whereas the second process needs this energy to transport specific substances. The present work is focused on the study of ion channels, and in particular the facilitated diffusion mechanism of ion transport across the membrane proteins. The next section will concentrate on this mechanism.

1.1.1 Facilitated diffusion mechanism

From a thermodynamic point of view, the cell membrane behaves as a selective boundary between two compartments with different ionic concentrations (K^+, Cl^-, Na^+, Ca^{2+}). For a better understanding of the thermodymamic processes, the membrane and the internal plus external compartments will be refered to as a *system*. Therefore, the variables that can affect the balance of the system would be limited to the number of a given type of ionic particles in each compartment (N_i) and the difference of potential ($\Delta\Psi_i$) generated, due to the tendency of ions or polar molecules to diffuse in response to a concentration gradient. The Gibbs equation $G(T, P, N, \Psi)$ for each type of ion (i) in laboratory conditions (tempera-

ture, volume and pressure constant) can be expressed by:

$$dG = \sum(\mu_i dN_i) + \Psi dq_i \tag{1.2}$$

where μ_i is the chemical potential associated to a given ionic species i and q_i the charge. If the variation in charge is expressed by

$$dq = z_i F dN_i \tag{1.3}$$

where z_i is the valence of i and F is the Faraday constant, the Gibbs equation in (1.2) for each kind ion species can now be written:

$$dG_i = (\mu_i + z_i F\Psi)dN_i \tag{1.4}$$

where $(\mu_i + z_i F\Psi)$ is defined as *the electrochemical potential* $\bar{\mu}_i$ for a given ion species i. It is the driving force associated to a change in the number of charged particles. In conditions where an ion (i) crosses the membrane from the internal compartment to the external compartment in response to a concentration gradient ($\Delta\mu = \mu_i^{\text{ext}} - \mu_i^{\text{int}}$) and/or a difference of potential ($\Delta\Psi = \Psi_i^{\text{ext}} - \Psi_i^{\text{int}}$), the system will be at equilibrium ($dG = 0$) when:

$$\mu_i^{\text{ext}} - \mu_i^{\text{int}} = z_i F(\Psi_i^{\text{ext}} - \Psi_i^{\text{int}}) \tag{1.5}$$

If in the equation (1.4) the chemical potential is expressed in terms of ionic concentration species i, one obtains the *Nernst equation*:

$$\Psi_i^{\text{ext}} - \Psi_i^{\text{int}} = -\frac{RT}{z_i F} Ln \frac{[C]_{\text{ext}}}{[C]_{\text{int}}} \tag{1.6}$$

This equation accounts for the value of the electric potential at which the ion flow ceases.

In biological environments, impermeable cytosolic molecules such as proteins are negatively charged so that an electrochemical gradient is always present. The system goes to a stationary equilibrium called *Gibbs-Donnan equilibrium*, where the system must meet the following conditions:

- Electroneutrality: In each side of the membrane the number of negative particles must be equal to the number of positive particules.
- The net flow of all the diffusible ions across the membrane become zero and a membrane potential is given according to the ionic species concentrations and their respective permeabilities.
- Osmotic balance: Water molecules move passively across of membrane following their chemical gradient and an osmotic pressure is generated. When the water molecules move into the cell, the cellular volume can be maintained by different action mechanisms which require the metabolic energy (*active transport*) and/or passive transport the ions and solutes molecules across of the membrane.

In the early period of classical biophysics, scientists such as Alan Hodgkins and Andrew Huxley proposed that the action potential in nerves impulse and other electrical signals in excitable cells were due to variations in membrane potential caused by changes in ionic permeability. These results were obtained without complete knowledge of the molecular structure of the membrane proteins involved. Now it is known that different membrane proteins are involved in the generation of the action potential and that the behavior of their molecular structure regulates this process. Structure-function features are strongly related to the role of proteins

in the cells. Therefore, the knowledge of the structure of proteins and their molecular interactions allow us to understand their possible functions and regulatory mechanisms.

1.2 Protein structure organization levels

All natural proteins consist of L-amino acids (L-aa) chains, where each amino acid structure consists of a carbon called *alpha carbon* C^{α} to which attached an hydrogen atom, an amino and carboxylate groups, and a chemical group R, called *side chain* or *residue*(figure 1.1a). The side chain compound confers to the amino acid his specific physical and chemical properties. The L-aa are linked by an amide bond. The carboxyl group of one amino acid reacts with the amino group of another amino acid, and this reaction releases one water molecule and generates a planar amide bond between the amino-acids, known as *peptide bond*.

The amino acid sequence of residues that constitutes a protein is called *primary structure* (figure 1.2b). This structure can not give, however, the information of spatial protein distribution therefore tostructure can not give, however, informations about of spatial protein distribution. In order to determine the structural and functional properties of the proteins, it is necessary to know how residues are in contact each other.

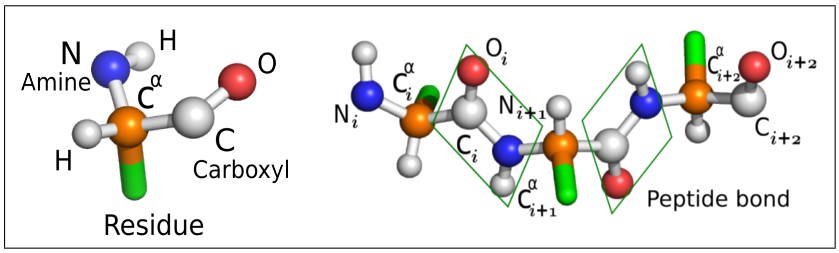

Figure 1.1: Essential units of the formation of proteic structure. (Left) L-amino acid composition. (Right) Peptidic bond joining two amino acids.

In the 1950s, research involving quantum mechanics calculations and X-ray

patterns using oligopeptides determined the spatial parameters that characterize peptide bond length and rotations around the C^{α}. Two successive peptide bonds between three amino acids are shown in the figure 1.2. Each peptide bond containing the O_{i-1}, C_{i-1}, N_i and H_i atoms is planar. Similarly, the junction of the ith and $(i+1)$th amino acid creates the second planar peptide bond containing O_i, C_i, N_{i+1} and H_{i+1} atoms. The stiffness of movement of a peptide bond arises from the torsion angle between C - N bond (ω), which never differs too much from 180°. It is possible to find two additional rotations around the N_i - $C_i{}^{\alpha}$ (the amide nitrogen and α carbon) and $C_i{}^{\alpha}$-C_i (carboxyl and α carbons) bonds, defined by the dihedral angles ϕ_i and ψ_i respectively. The backbone of a protein can be described by the C^{α} positions ϕ_i and ψ_i parameters. Side-chain configurations of a protein will be detected by the degrees of freedom of rotation (*rotamers*).

Linus Pauling and coworkers in 1951 proposed a new secondary structure organization in proteins. They thought that if the planar peptide bond property is kept in tridimensional structure of proteins, a helical conformation (α helix) is possible to form, where the axial distance between two successive residues is 1.5 Å, the rotation angle is 100°and where the values of ϕ and ψ dihedral angles correspond to -57°and -47°respectively. A turn of the helix contains 3.6 peptide units and a hydrogen bond is formed between donor and acceptor which are separated by four residues $i \rightarrow i+4$. Other different types of secondary structures were defined in proteins by identification of their hydrogen bonds and ϕ and ψ values.

The secondary structure of a protein is stabilized by the formation of the *hydrogen bond patterns* between the amide hydrogen (N-H) atom of the amide group with the carbonyl oxygen (C=O) atom of the carboxyl group in the same main chain or between the atoms of the two parallels chains (figure 1.2). Table 1 describes the most probable protein secondary structure conformations based on the Kabsch and Sander's algorithm, which defines the secondary structure of protein

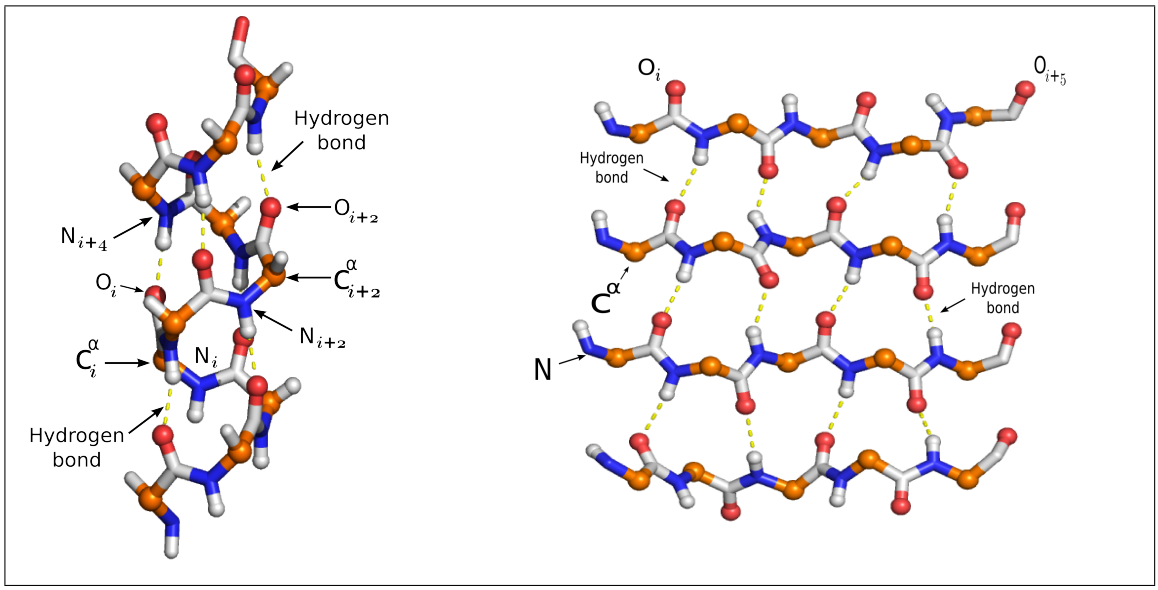

Figure 1.2: Primary structure arrengements of proteins. (Left) α-helix and (Right) Parallel β-sheet.

(*DSSP*) from the crystalographic atomic coordinates(PDB file)(Kabsch W, 1983).

Structure	ϕ (°)	ψ (°)	Number of residues per turn	Distance between peptide units
α helix	-57	-47	3.6	1.5
3_{10} helix	-49	-26	3.0	2.0
π -helix	-55	-70	4.4	1.15
Parallel β -sheet	-119	113	2	3.25
Anti-parallel β -sheet	-139	135	2	3.47

Table 1.1: Main Features of the common secondary structure in proteins.

There is also an alternative way to visualize the secondary structure developed by et al (1963). They considered the atoms as hard spheres with radius equal to van der Waals radii. The dihedral ψ and ϕ angles conformations of experimental polypeptide structures were plotted in a 2D plane, that defines different regions which characterize secondary structure conformations. Figure 1.3 shows the white areas corresponding to conformations where atoms in the polypeptide come closer than the sum of their van der Waals radii. These regions are sterically disallowed

for all amino acids except glycine which is unique because it lacks a side chain (it has an hydrogen atom).

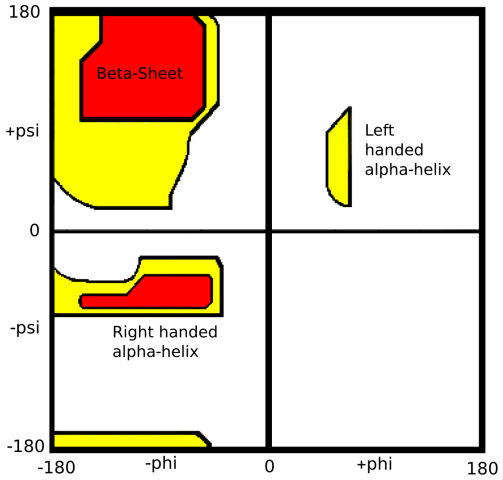

Figure 1.3: Ramachandran diagram of the possible dihedral angles conformations to the secundary structure of a protein.

The red regions in the figure correspond to conformations where there are no steric clashes, for example, these are the allowed regions referring to the α helical and β sheet conformations. The yellow areas show the allowed regions if slightly shorter van der Waals radii are used in the calculation, the atoms are allowed to come a little closer together.

Proteins can have many regions with different secondary structures. For example, the transmembrane segments of *ionic channels* are formed of α helices but the channel cytosolic regions can have a variety of local conformations that contain β and α helices. The overall organization of local conformations (spatial relationship) generates the *tertiary structure*. This structure can be stabilized by also hydrogen bonds, salt bridges, disulfide bonds or hydrophobic interactions. The new structural organization allows proteins to perform specific physiological functions such as enzymatic reactions or molecular transport. When the function is

performed by an ensemble of proteins, this complex structure is called *quaternary structure* and each protein constituent is called a *subunit*.

1.3 The ionic channels

Ionic channels are integral membrane proteins which use the ions electrochemical gradient to ensure ionic transport. They are formed by oligomeric complexes of several subunits. Most channels have three, four, or five homologous or identical subunits, arranged in circular symmetry, forming a single aqueous pore. However, one set of chloride family channels (*ClC*) has two pores per channel (Hille, 2001). Ionic channel proteins can be permeable to anionic or cationic ions. Some channels, however, are not selective and can not distinguish between negative and positive ions. Ion channels can discriminate between ions with highly similar chemical structures. For example, some potassium channels are about 10000 times more permeable to K^+ than to Na^+, while maintaining a high diffusion rate of $10^6 ions/s$. Today, it is known that a "signature " amino acid sequence in the channel structure accounts for the selectivity to ions (Heginbotham et al., 1992) so, permeability and selectivy properties of the ions channels are intrinsically linked to the structure-function of each channel.

Channel proteins' behavior is characterized by a property called *gating*, which refers to the ion channel capacity to fluctuate between two states that allows or disallows the diffusion of ions. Gating is a dynamic process that involves various structural reorganizations of the protein, achieving a non-conducting (closed state) or a conducting state (open state). When the channel is in the open state, the ions diffuse through the protein randomly and the transition to a close state is driven

by thermal fluctuations (Weiss, 1996). Conductance and gating mechanisms are other molecular properties used to classify many kinds of channels.

Channel expression and localization into the cell membranes also constitute another important property of the channels that contribute to the physiological function response. For example, in epithelial cells, Cl^- channels which are localized at the apical side of the cell play an important role in transporting Cl^- ions, while in excitable cells they maintain the membrane potential. Na^+, K^+ channels are necessary to perform action potentials in excitable cells. For example, the nerve conduction in the giant axon of the squid starting by a stimulus that allows that the resting membrane potential go throught to more positive membrane potential and open the Na^+ channels. The Na^+ influx depolarizes cell membrane at positive values, near of the Na^+ potential equilibrium (E_{Na^+}) and in this conditions, the K^+ channels in the membrane giant axon are opening while $Na+$ channels are inactivated. The outward flux of the K^+ ions repolarize the membrane potential leanding it to an hyperpolarization state. Na^+, K^+ and Ca^{2+} channels also are essential for rapid calcium intracellular signaling pathways and cell to cell communication. The next section describes the general structural features of the K^+ion channel superfamily.

1.4 The Potassium ionic channels

Potassium ion channels form the major superfamily of channels present in both procaryotic and eucaryotic cells, they are responsible for great diversity of functions such as modulation of electrical activity and intracellular pH. Mutations of the potassium channel genes are associated to neurological, cardiac and vascular

diseases. Regulation of the cellular K^+ channels expression on different tissues on mammalian cells can also effects in volume and cell proliferation.

The name of potassium ion (K^+) channels is due to their main function; they show a higher selectivity for the transport of K^+than to other monovalent cations. Studies on the permeability of potassium channels have shown a selectivity sequence ($K^+ \sim Rb^+ > Cs^+$) among ions with similar radius as K^+, while for small monovalent alkali metal ions such as Na^+ and Li^+, the permeability is smaller ($P_{Na} \ / \ P_K < 0.01$) (Hodgkin and Keynes, 1955). K^+ channels are integral membrane proteins formed by an assembly of transmembrane helices (TM), which are associated to constitute a functional channel. Each channel is formed from 4 subunits composed of 2, 6 or 7 TM helix segments (S1-S6,S0). Crystal 3-D structures of these channels show that the selective filter region (TXGYG) is located in the external segment of the pore and is connected to the pore helix and the transmembrane α helix, which forms the pore lumen (M2 or S6 segments nomenclature) (Doyle et al., 1998).

K^+channels can be classified according to the mechanism of *activation* or *gating*. There are K^+ channels whose activation is due to variations in membrane potential. These channels are known as *voltage-gated*. Voltage-gated channels are built from four homologous subunits, each comprising a voltage-sensor domain and a pore-forming domain. In eukariotic cells, the *Shaker*-related subfamily $K_v\alpha 1.x$ is the most known. There are other types of K^+channels which are activated by extracellular ligands such as ACh (K_{Ach} channels) or by intracellular ligands such as Ca^{2+} (K_{Ca} channels), intracellular pH (KcsA bacterial channel) or by internal nucleotides like cAMP (Hille, 2001). K^+channels can also contain transmembrane, external or intracellular auxiliary subunits (called e.g. β, δ, γ) which play different functional roles in K^+channels. For example, in voltage-gated channels, the $K_v\beta$

subunit confers a fast inactivation kinetics which play a key role in pre and postsynaptic nervous signal generation (Rettig et al., 1994). In K_{ATP} channels the binding of sulfonylureas agents such as glibenclamide to the auxiliary subunit (*SUR*x) inhibits channel activity (Doyle and Egan, 2003) and in some K_{Ca} channel subfamilies ($K_{Ca}2.x$ and $K_{Ca}3.1$), the Calmodulin (CaM) β subunit is crucial for cell surface expression and gating (Lee et al., 2003).

1.5 The calcium activated potassium channel family

Based on their single channel conductance, genetic relationship and mechanisms of Ca2+ activation, the eight K_{Ca} channels identified so far form two well-defined groups. The first group contains the $K_{Ca}1.1$, $K_{Ca}4.1$, $K_{Ca}4.2$ and $K_{Ca}5.1$ channels characterized by rather large unit conductance (>100 pS). The best-studied channel of this group is $K_{Ca}1.1$ (MaxiK) (Eisenman et al., 1986), which is both voltage and Ca^{2+} sensitive, and known to be critical to vascular smooth muscle cell contraction (Latorre et al., 2000). The $K_{Ca}2.x/3$ group refers to the three small conductance channels, ($K_{Ca}2.1$, $K_{Ca}2.2$ and $K_{Ca}2.3$ and to the intermediate conductance $K_{Ca}3.1$ channel), which are voltage insensitive and are activated at intracellular calcium concentrations $[Ca^{2+}]_i < 1.0$ μM (Kohler et al., 1996). These channels are present in a wide range of excitable and non-excitable cells and are involved in intracellular calcium signaling cascades. $K_{Ca}2.x$ channels are mainly expressed in the nervous system and they are involved in the modulation of neuronal firing properties (Kohler et al., 1996), while $K_{Ca}3.1$ channel is mostly expressed in blood and ephitelial cells and in some peripheral neurons such as the neurons of the myenteric ganglia in Crohn's bowel (Hesse et al., 2003). Table 1.2 presents a comparative description of the main features between BK_{Ca}, SK_{Ca} and $K_{Ca}3.1$ channels.

The other K_{Ca} channels ($K_{Ca}4.x$ and $K_{Ca}5.1$) are not presented as they are activated by Na^+ ions.

The genes that encode the three SK_{Ca} and $K_{Ca}3.1$ channels belong to the *KCNN* gene family (Kohler et al., 1996). An homology analysis of their primary structures showed poor sequence identity (< 40 %) for the S1-S4 TM segments and the intracellular N-terminus region. In contrast the core domain S5-pore-S6 is highly conserved as every selective K^+ ion channels. To date, there is not a crystal structure of the pore region. Studies using cysteine mutagenesis analysis and computer models suggest that the activation gate is located in the channel deep cavity near the selectivity filter or perhaps in the selectivity filter itself (Simoes et al., 2002; Bruening-Wright et al., 2007; Garneau et al., 2009). Furthermore, the gating in SK_{Ca} channels and $K_{Ca}3.1$ channels is coupled through an association with the intracellular β subunit CaM (Xia et al., 1997; Keen et al., 1999). Early fluorescence measurement studies reported two CaM binding domains (CaMBDs) responsible for constitutive and Ca^{2+}-dependent interactions between CaM and SK_{Ca} channels (Keen et al., 1999).

In 2001, Schumacher and coworkers obtained a crystal structure at 2.9 Å resolution (PDB:1G4Y) of the SK_{Ca} 2.2/Ca/CaM/ complex from the rat SK_{Ca} 2.2 channel (Schumacher et al., 2001). The X-ray structure showed a CaM C-lobe constitutively bound at the membrane proximal intracellular region (413-440) of the SK_{Ca} 2.2 channel and a Ca^{2+}-dependent CaM N-lobe making contact with both CaMBD domains. On the basis of this structure, a chemomechanical gating model was proposed where a large-scale conformational rearrangement would be taking place in the presence of $Ca^{2+}$when the N-lobe of CaM binds to a C-terminus segment of an adjacent channel monomer resulting in a dimerization of two contiguous subunits (Schumacher et al., 2001, 2004). This rearrangement allows a rotation / translation of the associated S6 transmembrane domains resulting in a structural reorganiza-

FEATURES	$SK_{Ca}(2.x)$	$K_{Ca}3.1$	$BK_{Ca}1.1$
Number of AA (Human)	543, 579 and 736 respectively	427	1822
Number of TM	6	6	7
Subunits Associates	Calmodulin (CaM)	Calmodulin (CaM)	Slo1 (TM) Slo-β_1
Calcium Dependance	Ca^+ binding CaM at C-terminal	Ca^+ binding CaM at C-terminal	Intrinsic Ca^+ binding C-terminal
Voltage Dependence	None	None	Yes
Single channel Conductance	9-18 pS	20-80 pS	100-250 pS
Maximal open probability (Po_{max}) in $[Ca]_i$ saturated	0.8 5 μM	0.46 (at 40 mV) 10 μM	0.2 without ATP 25 μM
Inhibitor Compounds	Apamin(nM) Scyllatoxin(nM) d-Tubocurarine (μM)	TRAM-34(nM) ICA-17043 (nM) Charybdotoxin (nM)	Iberiotoxin TEA (mM) Paxilline
Enhancer and opener Compounds	1-EBIO, NS309 riluzole	1-EBIO, DCEBIO riluzole methylxanthine	NS1608, NS1619 DHS-1, estradiol BMS204352
Tissue or cell localization	Central and peripherical nervous system endothelial cells	smooth muscle, mitochondria, blood red and tumour cells epithelial cells endothelial cells	Heart, Brain skeletal muscle, mitochondria

Table 1.2: Principal properties of the BK_{Ca}, SK_{Ca} and $K_{Ca}3.1$ Ca^{2+}-activated dependent K^+channels. Data information extracts from (Chris et al., 1998; Pedarzani and Stocker, 2008).

tion of the pore residues at the channel gate in the selective filter or close to it.

The $K_{Ca}3.1$ CaMBD regions present an high amino acid sequence identity with SK_{Ca} channels ($> 84\%$). However in contrast to SK_{Ca} channels, $K_{Ca}3.1$ is also regulated by internal ATP through a phosphorylation related process. This activation effect requires the presence of intracellular Ca^{2+}ions (Gerlach et al., 2001; Srivastava et al., 2006). Pharmacologically, SK_{Ca} and $K_{Ca}3.1$ can be easly distinguished: $K_{Ca}3.1$ is insensitive to the specific SK_{Ca} channel blocker apamin (see table 1.2), but it is affected by blockers and toxins such as TRAM-34, Maurotoxin and Charybdotoxin which do not affect SK_{Ca} channel activity (Wulff et al., 2007).

In our laboratory we are interested in the biophysical structure-function relationships of the $K_{Ca}3.1$ Ca^{2+}-activated K^{+}channel in epithelial and endothelial cells. In this work we wish to provide more evidence for a modulation of the $K_{Ca}3.1$ gate by Ca^{2+}- CaM binding to the channel.

1.6 The intermediate conductance Ca^{2+}-activated K^{+}channel: KCa3.1

1.6.1 Physiological implication of KCa3.1 channel in non excitable cells

The voltage insensitive Ca^{2+}-activated K^{+}channel of the intermediate conductance $K_{Ca}3.1$ was first characterized in red blood cells in 1958, in these studies G. Gárdos found that K^{+}currents elicited in human erythrocytes were dependent on intracellular Ca^{2+}. This studies allowed the first link between Ca^{2+}signaling cascades and K^{+}membrane permeability (Gardos, 1958). $K_{Ca}3.1$ was later cloned in 1997 from human pancreas by the Ishii's group (designated hIK1)(Ishii et al., 1997). They detected by Northern blot analysis and electophysiological techniques

that hIK1 is expressed in several peripheral body tissues such as the bladder, thymus and colon, but not expressed in the brain. Currently it is known that the $K_{Ca}3.1$ channel is also expressed in microglia cells (Kaushal et al., 2007). $K_{Ca}3.1$ is involved in a large variety of health disorders, from angiogenesis disorders to volume regulation in blood cells. Table 1.3 summarizes some of the important diseases, tissue or cell expression localization and possible treatments that have been documented for $K_{Ca}3.1$.

Health Disorders	Tissues or cell expressions	Treatments	References
Sickle cell Anaemia	Blood red cells	Inhibition $K_{Ca}3.1$ by ICA-17043 or Clotrimazole	Chandy et al. (2004) Stocker et al. (2003)
Immunomodulation and Autoimmunitary diseases	Naive T_{CM} cells Naive IgD^+ $CD27^+$ and B memory cells	Inhibition $K_{Ca}3.1$ T_{CM} non activated Inhibition $K_{Ca}3.1$ After B cells activation	Wulff et al. (2004)
Retinal Degeneration	Ganglion cells	Inhibition $K_{Ca}3.1$ by TRAM-34	Kaushal et al. (2007)
Hypertension and Retenosis	Vascular endothelial cells	Activators $K_{Ca}3.1/K_{Ca}2.3$ NS309/Aminopiridine	Si et al. (2006) Sankaranarayanan et al. (2008)
Atheroscleric vascular disease	VSMC,macrophages and white boold cells	Inhibition $K_{Ca}3.1$ TRAM-34 and Clotrimazole	Toyama et al. (2008)
Cystic Fibrosis	Airway epithelial cells	Openers EBIO, CBIQ Chlorzoxazone	Devor et al. (1996) Gao et al. (2001)
Asthma	Human Lung mast cells	Blockade $K_{Ca}3.1$ by chemotatic stimulus (CXCL10)	Cruse et al. (2006)

Table 1.3: Important diseases associated to $K_{Ca}3.1$, localization and possible treatments.

Besides the biochemical and electrophysiological research where $K_{Ca}3.1$ plays

an important role in pathological conditions, the study of $K_{Ca}3.1$ on knockout mice showed a significant implication of this channel in the regulation of total peripheral vascular resistance. The lack of the $K_{Ca}3.1$ gene and consequently the loss of KCa3.1 currents, results in an impaired Endothelial-derived hyperpolarizing Factor (EDHF) -mediated smooth muscle dilation and elevated systemic blood pressure (Si et al., 2006).

In microvascular endothelial cells (EC), EDHF is characterized by the combination of the vascular smooth muscle cells (VSMCs) and endothelial cells resulting in a vasorelaxation. Currently this effect is not completely understood. Hyperpolarization of the endothelial cells can be caused by shear stress or agonists that stimulate G protein-coupled receptors which increase intracellular Ca^{2+}concentration and cause endothelial membrane hyperpolarization via $SK_{Ca}2.3$ and $K_{Ca}3.1$ activation (figure 1.4). There are two consequences to the hyperpolarization of EC, namely: nitric oxide (NO) generation and augmentation of K^{+}ions in the intercellular cleft near the VSMCs (Edwards and Weston, 2004). Additional studies have also provided evidence for an electrical coupling between the endothelium and the adjacent vascular smooth muscle cells via myoendothelial gap junctions (Griffith, 2004). Hence a possible EDHF -mediated VSMCs hyperpolarization could arise from the direct electrical gap junction coupling and/or accumulation of extracellular K^{+}ions evoked for $K_{Ca}3.1$ in the restricted space surrounding the myoendothelial gap (Félétou and Vanhoutte, 2007). K^{+}ions would then hyperpolarize the VSMC by activating the potasium KIR smooth muscle channels and/or Na^{+}/K^{+}pump (Edwards and Weston, 2004; Félétou and Vanhoutte, 2007), and close L-type voltage gated Ca^{2+}channels, thereby decreasing the intracellular Ca^{2+} (Yamamoto et al., 1999)(see figure 1.4). Therefore, abolishing the endothelial $K_{Ca}3.1$ currents can cause a reduction of endothelial and smooth muscle hyperpolarization.

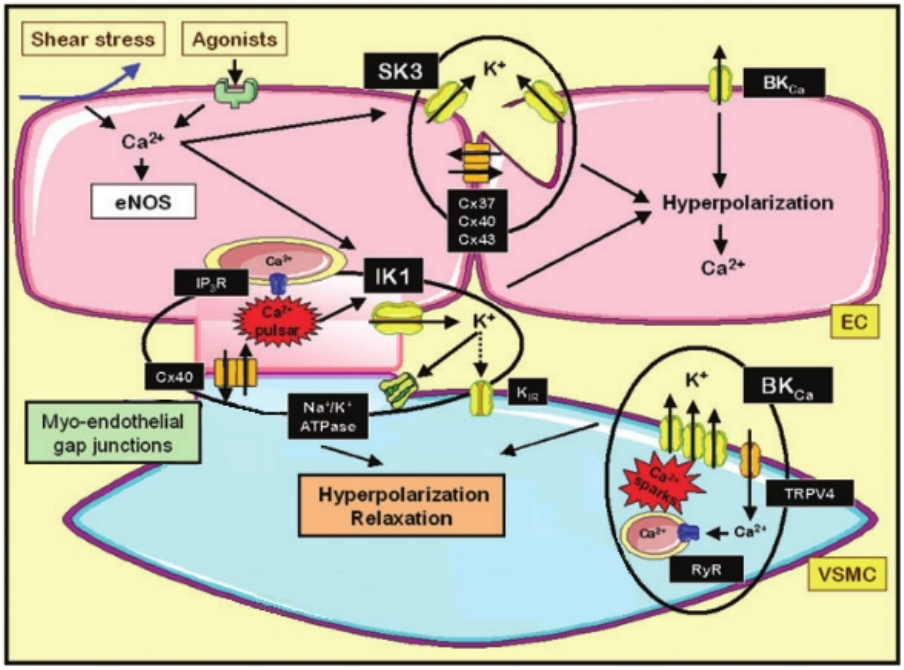

Figure 1.4: Physiological implications of $K_{Ca}3.1$ in signaling of possible pathways of Endothelial-derived Hypolarizing Factor (EDHF). Adapted from (Sheng et al., 2009)

Recent data have also indicated that $SK_{Ca}2.3$ and $K_{Ca}3.1$ activators (NS309 and DCEBIO respectively) could enhance cytosolic Ca^{2+}transients and acute NO synthesis in isolated endothelial cells (Sheng et al., 2009). These results show that the endothelial $K_{Ca}3.1$ channel is a fundamental determinant of endothelial hyperpolarization and EDHF signaling and, thereby, a crucial determinant in the control of peripherical microcirculation. Structural molecular studies become, however, essential to understand how selective molecules can modulate channel activity thus providing the novel therapeutic approaches for the treatment of cardiovascular diseases.

1.6.2 Regulation

In addition to Ca^{2+}sensitivity, $K_{Ca}3.1$ is also modulated through kinases and phosphatases. As previously mentioned, $K_{Ca}3.1$ can be activated by ATP whereas hSK1,

rSK2, and rSK3 are ATP insensitive. The ATP dependence region in $K_{Ca}3.1$ was early identified using h$K_{Ca}3.1$/r$SK_{Ca}2.2$ chimera; a 14 amino acid region extending from Arginine 355 to Methionine 368 residues in the C-terminus domain of $K_{Ca}3.1$. The same region has also been shown to interact with calmodulin in a Ca^{2+}- dependent manner (Gerlach et al., 2001). Studies performed by Srivastava and coworkers (Srivastava et al., 2006) on a CD4 T cell expression system, provided evidence for a regulatory effect by the nucleoside diphosphate kinase B (NDPK-B) of the ATP phosphorylation dependent activation of endogenous $K_{Ca}3.1$ channels. NDPK-B is a mammalian histidine kinase which binds and activates $K_{Ca}3.1$ by phosphorylating the histidine 358 at the C-terminal region of the channel. The stimulatory action of ATP required Ca^{2+}leading to an apparently greater Ca2+ sensitivity.

Another specific regulatory effect of $K_{Ca}3.1$ channels in CD4 T-cells activation was reported recently: the class II phosphatodylinositol-3 kinase C2β (PI3K-C2β) regulates channel activity via the indirect action of the phosphatidylinositol-3 phosphate (PI(3)P) in the C-terminal region (355-369) of the $K_{Ca}3.1$ channel (Srivastava et al., 2009). The PI(3)P phosphatase myotubularin-related protein 6 (MTMR6) and the histidine phosphatase, phosphahistidine phosphatase-1 (PHPT-1) were identified as negative regulators of the $K_{Ca}3.1$ channel by dephosphorylating PI(3)P (Srivastava et al., 2006). It was hypothesized that PI(3)P facilitates the Ca^{2+}dependent binding of CaM to $K_{Ca}3.1$ via the recuitment of a regulatory subunit. Other results from Devor's laboratory suggest that the multi-basic RKR motif in the N-terminal domain of the $K_{Ca}3.1$ would be involved in the phosphorylation of the H358 residue too. The RKR/AAA mutation in the N-terminal region of the channel did not alter the Ca^{2+}dependent gating of $K_{Ca}3.1$ but this mutation abolishes the ATP-dependent activation of $K_{Ca}3.1$ (Jones et al., 2007). PKA has also been documented to regulate the human KCa3.1 channel, but it is currently believed

that K_{Ca}3.1 is not itself a target of PKA, because mutations of the PKA-consensus sites in the human KCa3.1 affected neither the basal nor the ATP-activated current Gerlach et al. (2000, 2001). Work from our laboratory has also provided the first evidence for the C-terminal region of K_{Ca}3.1 (380-400) interacting with the γ 1- subunit of the metabolic sensing kinase AMPK. Notably, channel activity was found to decrease in response to AMPK stimulation, arguing for a complex regulation of K_{Ca}3.1 by protein kinases (Klein et al., 2009). Altogether, these observations point toward a complex ATP-dependent regulation of the KCa3.1 channel activity that could involve multiple intracellular sites and/or several ATP-sensitive auxiliary proteins.

1.7 Structural molecular studies of the KCa3.1 channel

To better understand the functional and structural molecular relation of the K_{Ca}3.1 channel, our laboratory has cloned the K_{Ca}3.1 channel from Hela cells by polymerase chain reaction (PCR) using two oligonucleotides designed from the reported hKCa4 sequence (EMBL/ GenBank/DDBJ accesion no. AF022150). Sequencing the PCR product obtained from Hela cells revealed a 100% identity with the sequences reported for the hKCa4 and hSK4 (EMBL/GenBank/DDBJ accesion no. AF000972). The resulting gene product was identified as an intermediate conductance K^+channel (IK_{Ca}) based also on the pharmacological and electrophysiological property studies in Xenopus oocytes (Simoes et al., 2002). The DNA of the KCa3.1 channel encodes for a protein composed of the 427 amino acids organized in six transmembrane segments S1-S6 with a single pore motif between segment 5 (S5) and 6 (S6) similar to the voltage-gated family of the K^+channels. Adjacent to the pore K_{Ca}3.1 there is a putative N-linked glycosylation site. The intracellular N-terminus is composed of only twenty four amino acids but it contains a

multi-basic RRRKR and leucine Zipper (LZ) motifs which are critical for channel assembly and trafficking (Jones et al., 2004) (figure 1.5).

Besides the CaM binding domains at C-terminus, $K_{Ca}3.1$ presents an other LZ region (378-406), essential for the correct folding and cell surface expression at the membrane plasma. Double mutations of leucines L396A/L403A in this region completely abrogated $K_{Ca}3.1$ membrane localization (Syme et al., 2003).

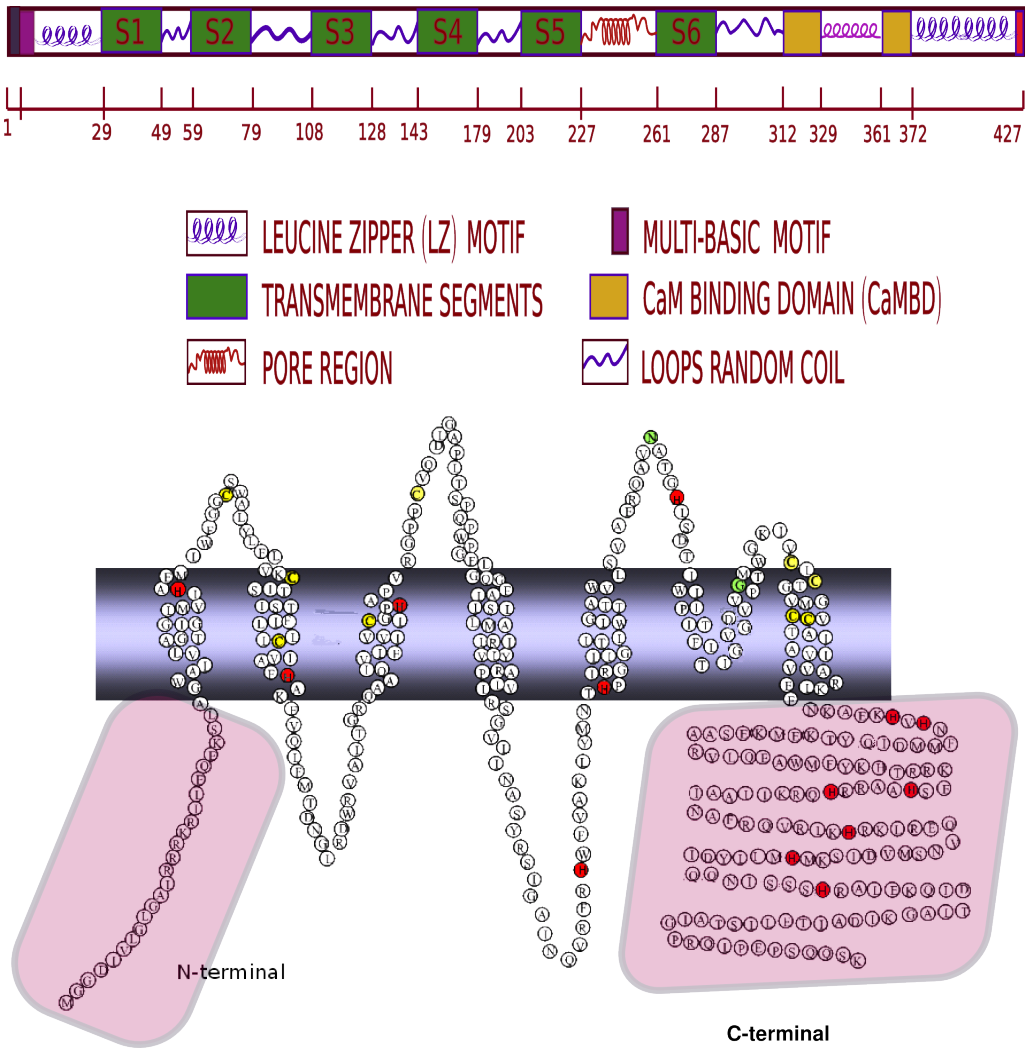

Figure 1.5: Linear and topological representations of the KCa3.1 potassium channel. The membrane topology predicts that 7 of the 13 His residues (red colour) are part of the C-terminal domain. Cystein residues are coloured in yellow.

1.7.1 Model of the gating mechanism in $K_{Ca}3.1$ channel

Even though the crystal structures of the conduction domains of different K^+ channels and the Ca^{2+}/CaM/ channel complex structure of the rat $SK_{Ca}2.2$ have been resolved, the gating mechanism and the gate localization of $K_{Ca}3.1$ remain controversial. Our laboratory in the last decade has provided key molecular descriptions of the open/closed $K_{Ca}3.1$ pore region and the possible residues at the S6 transmembrane segment of $K_{Ca}3.1$ which can be involved in the channel gating process. 3D structure of the S5-Pore-S6 region of $K_{Ca}3.1$ in close and open configurations were generated by comparative protein structure modeling using the X ray structures of different K^+channnels such as: KcsA (PDB SeqID: 1f6g;1j95;1b18g), MthK (PDB:1LNQ) and the Kv1.2 structure (PDB:2A79) (Simoes et al., 2002; Klein et al., 2007). The models predict that residues T250, V275, T278 and V282 are projecting inside the pore lumen with C276 and C277 oriented opposite the pore (figure 1.6a). Analysis of the distance between S5-pore-S6 segment backbones of the opposite subunits in close and open configuration indicated that the inner vestibule dimensions of SK and Kv channels are conserved (Simoes et al., 2002). Also, individual cysteine mutagenesis from 275 to 286 residues were made and their reactivity with MTS compounds were registred by using the patch clamp technique in inside-out configuration. Rates of modification by $MTSEA^+$ application to the 275C (at the inner cavity) mutant channel showed no considerable differences between the channel's open and close states, whereas $MTSET^+$ modification resulted in rates 10^3 faster when applied to the open compared to the closed configurations. Additionally, residues located at the end part of the segment S6 of the $K_{Ca}3.1$ from A283 to A286 interacted with MTSET compound in absence of intracellular Ca^{2+}.

All these observations together suggest that: (1) The narrowest part of the conduction pathway should be located between the V278 and V282 residues and it is not obstructive to the passage of molecules with a volume less than MTSEA. (2)

although the inner cavity between SK and Kv is conserved, the bundle crossing structure formed by the intracellular end of the S6 segment does not have equivalent localization.

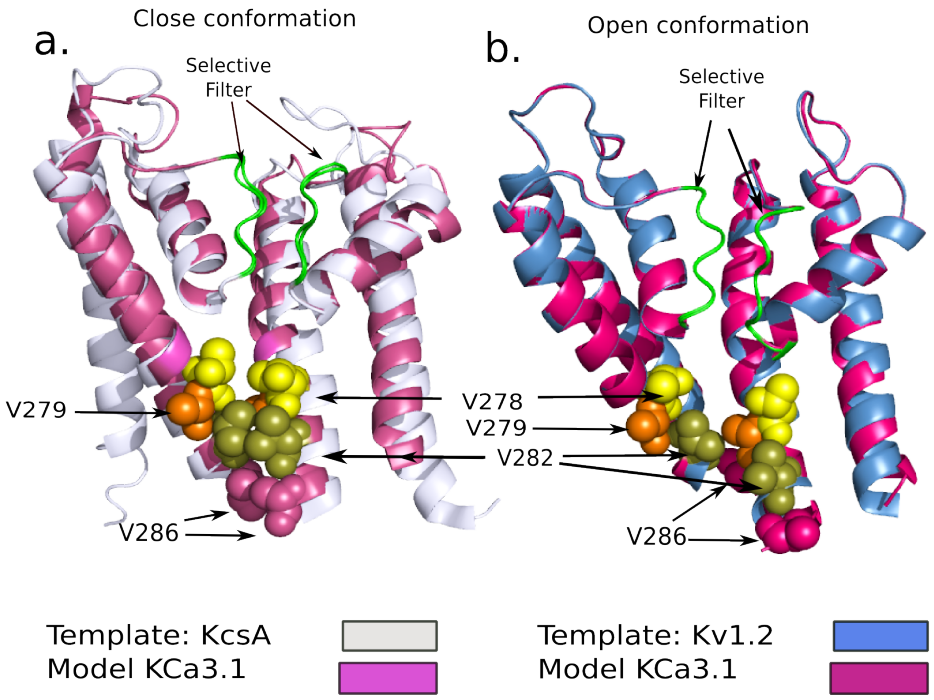

Figure 1.6: Lateral view of the transmembrane S5-pore-S6 segments of the $K_{Ca}3.1$ homology models (magenta) in close *a* and open *b* conformations. KcsA (grey) and Kv 1.2 (blue) structures were used as templates. Residues T278,V279 V282 of the $K_{Ca}3.1$ channel would be implicated in the sensor reception of the cytosolic conformation rearrangements at the CaMBDs regions when Ca^{2+}ion interacts with CaM.

Recent glycine (Gly) scanning experiments at the S6 segment of $K_{Ca}3.1$ made by our laboratory produced some $K_{Ca}3.1$ mutant channels which were constitutively active in zero Ca^{2+}(Garneau et al., 2009). Inside-out membrane patches of the A279G and V282G mutant channels presented current activity when they were exposed to bath solutions that were contained Ca^{2+} free (1 to 10 mM of EGTA in solution). Cysteine accessibility measurements to V275C in these mutants were also carried out using the sulphydryl reagents ($MTSEA^{+}$ and $MTSET^{+}$) and Ag^{+} ions. The results from these experiments strongly suggest that Gly mutant residues at positions 279 and 282 affect channel geometry in zero Ca^{2+}so that these channels

undergo less important structural changes as a function of Ca^{2+}concentration and that the hydrophobic interactions at 282 residue is critical in closing channel process (figure 1.6b).

Altogether, the gating model proposed by our laboratory is in agreement with a gate residing deep in the channel pore, in or close of the selectivity filter (Bruening-Wright et al., 2007). The hydrophobic interactions at V282 would favor S6 conformations that maintain the activation gate at the selective filter in a stable non ion conducting (close) configuration (Garneau et al., 2009). The binding of $Ca^{2+}$to CaM/K_{Ca}3.1 complex would induce a conformational change of S6 resulting in V282 being more exposed to water and the selectivity filter would transit into an ion conducting (open) state. This process accounts for the observation that the mutation of 282 by hydrophilic residues leads to channels that are constitutively open.

1.7.2 Toward a model of CaM-mediated gating in KCa3.1

As mentioned previously, K_{Ca}3.1 and SK_{Ca} gating requires the binding of $Ca^{2+}$to CaM constitutively bound to the channel C-terminus. The crystal and NMR structures of the CaM binding domain regions complexed with CaM in presence or absence of Ca^{2+}(called Ca^{2+}/CaM /CaMBD and apoCaM/CaMBD respectively) (Wissmann et al., 2002; Schumacher et al., 2001, 2004) have provided an important molecular insights on the interactions between the domains involved in SK_{Ca} gating.

The crystal structure obtained in the presence of calcium ions (PDB:1G4Y) showed that the Ca^{2+}/CaM/ CaMBD complex of the rat SK_{Ca}2.2 channel forms a dimer structure in which two antiparallel C-terminal segments of the channel are joined together by two CaM. In this configuration, one CaM interacts with three different α helices coming from two different α subunits (Schumacher et al., 2001) (figure

1.7a). Residues of the CaM binding domain (CaMBD1) proximal to the channel S6 segment interact with the decalcified C-terminal lobe *EF hand* pair of the CaM (C-lobe) while residues of the second binding domain (CAMBD2) make contacts with residues of the N-terminal lobe (N-lobe) of a second CaM molecule which contains two Ca^{2+}ions. Both lobes of CaM are connected by an extended unfolding central linker (figure 1.7a).

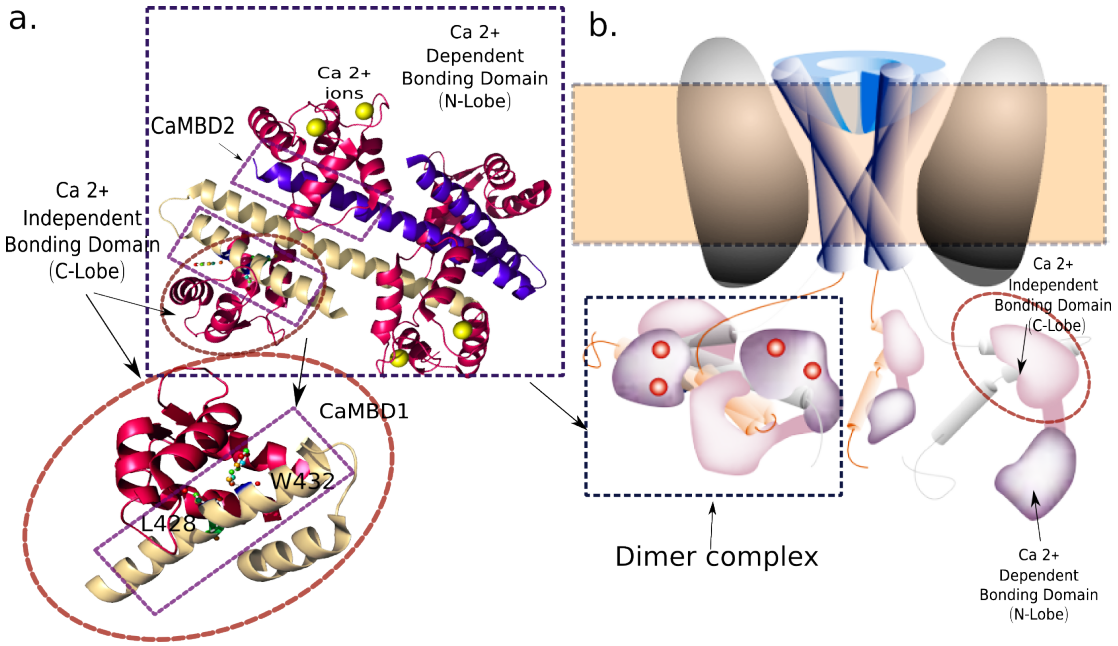

Figure 1.7: Ribbon and cartoon representations of the cytosolic dimer of the rat $SK_{Ca}2.2$ channel Ca^{2+}/CaM/CaMBDs complex. a. Ribbon representation of the crystal structure of the Ca^{2+}/CaM/CaMBDs complex (PDB:1G4Y) and the principal interactions between the proximal CaM binding domain (CaMBD1) residues (L428 and W432) of the $SK_{Ca}2.2$ with the pockets regions of the Ca^{2+}independent C-lobe of CaM. b. Cartoon model of the *sk*2 and $K_{Ca}3.1$ channels showed on the left the dimeric complex formation when Ca^{2+}ions interact with the Ca^{2+}dependent binding sites at the N-terminal lobe of the CaM. Figure adapted from (Yellen, 2001)

.

The C-lobe/CaMBD1 Ca^{2+}free complex is stabilized by several interactions involving three hydrophobic residues located inside three hydrophobic pockets of the C-lobe, with Ala425, Leu428 and Trp432 of CAMBD1 interacting with Phe89, Phe92 Leu105, Met109, Met124, Phe141 and Met144 of the CaM C-lobe. Only Leu428 is completely buried into the central hydrophobic patch (figure 1.7a).

The CaMBD2 extending from residue 473 to 483 includes the residues Leu480, Leu483 and Ala484 which upon Ca^{2+}binding are located inside the exposed hydrophobic N-lobe patch. These results showed that the interactions between the channel and CaM in the presence of $Ca^{2+}$are essentially hydrophobic. A recently, kinetic study of the N-lobe channel complex showed that when the N-lobe of CaM was left with only one functional ca binding site, the channel activity rapidly runs down but it was fast recovered by perfusion of CaM wild type protein or the same CaM mutant in the presence of the potent enhancer NS309 (Li et al., 2009). This result suggests that the N-lobe of calmodulin is also required for both SK channel gating and stable SK-calmodulin interactions.

An ApoCaM/CaMBD Ca^{2+}free crystal structure was also solved by the same group in 2004 (PDB: 1QX7). In these conditions all CaMBD segments presented a high degree of flexibility in comparison to Ca^{2+}/CaM/CaMBD complex and only a short segment of ten amino acids from the CaMBD was diffracted by X rays. These residues formed an α helix structure which corresponds to CaMBD1 (Schumacher et al., 2004). From a semi-open conformation in Ca^{2+}conditions, the C-lobe of CaM adopted a closed state in zero Ca^{2+}conditions, keeping only hydrophobic interactions with CaMBD1 residue Trp432. An interesting orientation change of the residues 430-440 as a function of Ca^{2+}led Schumacher and coworkers to suggest that the gating of SK_{Ca} K^{+}channels involves folding of the CaMBD which is induced upon binding of Ca^{2+}ions at the N-lobe of CaM which in turn is transmitted to the proximal CaMBD1, inducing a rotation of the pore located at the S6 segment of the channel (Schumacher et al., 2004) (figure 1.7b). Previous NMR spectroscopy studies of the ApoCaM/CaMBD support the key role of residues 430-440 of CaMBD1 in the Ca^{2+}independent interactions of the CaM with the channel (Wissmann et al., 2002). Notably, apoCaM/CaMBD complex showed less flexibility in solution in contrast to the crystal structure.

1.8 Objetives

The results obtained from x-ray crystallography support a role for hydrophobic residues in the Ca^{2+} independent interactions between CaM/CaMBD complex (Schumacher et al., 2001); however it remains unclear how Ca^{2+} binding to the N-lobe of CaM induces folding and dimerization of the channel C-terminus tails and translates into structural changes at selectivity filter to open the channel.

The present work concerns the structural basis by which calcium binding to the C-terminus of the CaM/K_{Ca}3.1 complex results in the opening of the channel gate at the level of the selectivity filter. Our approach consisted of: 1) Generating tridimensional structures of the Ca^{2+}/CaM/K_{Ca}3.1 C-terminal complex using as a template the X-ray structure obtained for the Ca^{2+}/CaM/SK_{Ca}2.2 complex (PDB:1G4Y). 2) Identifing the principal residues involved in the interactions between the Ca^{2+}/N-lobe/K_{Ca}3.1 complex. 3) Modifing the interactions between N-lobe/K_{Ca}3.1 complex by introducing Cysteine at specific locations (*SCAM*) and modification of the target Cys by methanethiosulfonate (MTS) reagents and finally analyzing how changing these interactions effects the equilibrium of the open gate probability or Ca^{2+}-dependence or both.

Chapter 2

Methodology

2.1 Computer-based Homology Modeling

3-D structures of the C-terminus region of KCa3.1 (D304-K373) and Calmodulin β subunit were generated through of a comparative protein structure modeling by the satifaction of spatial restraints method (Sali and Blundell, 1993). This method basically consists in four steps: (1) databank searching to identify structural homologues, (2) target-template sequence alignment in order to extract from the template structure homology-derived atom-atom distances and dihedral angles restraints, (3) model building and optimization, and (4) model evaluation. The crystal structure (1.6 Å resolution) of the C-terminal region of the rat $SK_{Ca}2.2$ channel (rSK2) was used as template (PDB:1G4Y) in agreement with the high amino acids sequence identity ($> 84\%$) obtained from the alignment analysis of the C-terminus region between *KCNN* subfamily channels (figure 2.1). The alignment analysis was calculated using the T-COFFEE multiple sequence alignment package available online at http://tcoffee.vital-it.ch/cgi-bin/Tcoffee/tcoffee_cgi/index.cgi .

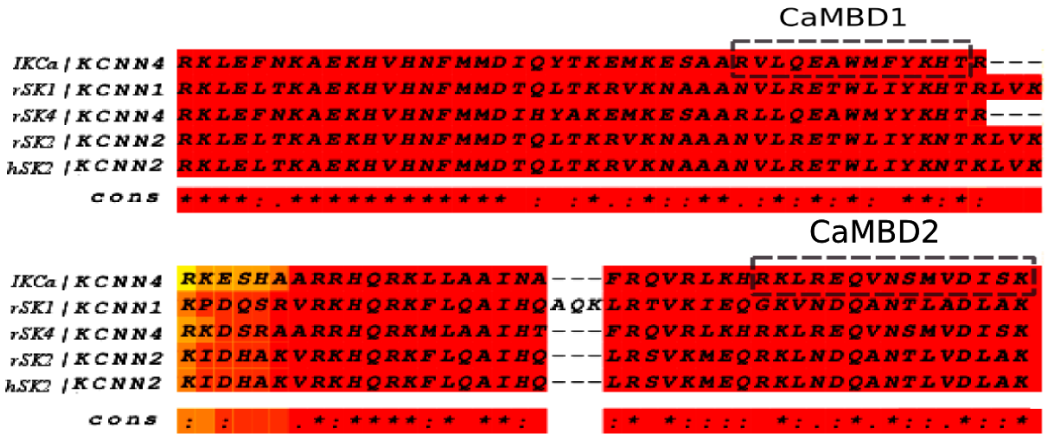

Figure 2.1: Multiple sequence alignments between calcium-activated $K^+SK_{Ca}2.1$, $SK_{Ca}2.2$ and $K_{Ca}3.1$ channels were performed with TCOFFEE package. Red color represents the high identity residues ($>$ 84%) and brown color medium residue identity(40%).

MODELLER 9v4 software which implements an automated approch to comparative protein structure modeling (Sali et al., 2001) was used to extract the spatial restraints for the cytosolic sequence D304-K372 of $K_{Ca}3.1$ channel and CaM (*target*) from the Ca^{2+}/CaM/CaMBD complex structure (*template*). One hundred structural models of $K_{Ca}3.1$ CaMBD domains and CaM protein were calculated and optimized by MODELLER minimizing as possible the violations on the spatial restraints. Ranking in model structures were based on a probability density function (PDFs) that accounts for the various structural features of the models. 14 models were selected based on their lowest PDF and Root Mean Square deviations (RMSD) between C^{α} of the models and the template. The model with lowest RMSD (1.8 Å) was kept and used as model structure of CaM/KCa3.1 complex. The overall structural quality of model was tested by PROCHECK.

2.2 Experimental Design

Model prediction was experimentally tested using the Substituted-Cysteine Accessibility Method (*SCAM*). Each residue of segment K360 - K373 at the C-terminus

of the KCa3.1 was mutated one at a time into a Cys and the susceptibility of the substituted Cys to reaction with charged or neutral methanethiosulfonate (MTS) reagents such as the positively charged $MTSET^{+}$, negatively charged $MTSES^{-}$ and neutral *MTSACE* reagents was measured; such a reaction forms a disulfide bond between a MTS molecule and the cysteine target. Binding rate depends on the hydrophobic environment of the target residue, with faster binding rate when the residue is in a water like environment and a slower rate when the residue is buried in a hydrophobic pocket (Akabas et al., 1992). MTS reagents were provided by Toronto Research Chemicals Inc. Site-directed mutagenesis was performed using the QuickChange site-direct mutagenesis kit (Stratagene).

SCAM effects of the K360 - K373 segment residues were recorded using the patch clamp technique in inside-out patch clamp configuration (Neher and Sakmann, 1976; Hamill et al., 1981). In this configuration the membrane patch is detached from the oocyte and the internal side of the membrane is exposed to the bath solution. Recording of currents was carried out using an Axopatch 200B amplifier (Axon Instruments, Inc) and digitized at a sampling rate 1 KHz with low pass filtering at 500 Hz. Patch pipettes were pulled from borisillicate capillaries using a Narishige pipette puller (model PP-83). Pipette resistance was between 2MΩ to 20 MΩ. Unless specified otherwise, the pipette potential was maintained at +60 mV throughout. Zero currents were recorded when patch membrane was exposed to the an EGTA containing solution with no Ca^{2+} added. Bath solution changes were performed using a RSC-160 rapid solution changer system (BioLogic Science Instruments). The solution exchange time was estimated to be less than 20 ms.

The pipette and bath solutions contained 200 mM K_2SO_4, 2.5 $MgCl_2$, 1 mM EGTA, and 25 mM HEPES plus $CaCl_2$ to yield a final free Ca^{2+}concentration of 25μM adjusted at pH 7.3 with KOH. Sultate salts were used to minimize the con-

tamination curent from the endogenous Ca^{2+}-dependent chloride channels. The free Ca^{2+} concentration solution was calculated using the EQCAL multiple equilibrium software (Biosoft, Cambridge, UK). To obtain a zero free Ca^{2+} solution (*EGTA*), 3 mM of EGTA was added to bath solution without $CaCl_2$ (estimated free Ca^{2+}<10 nM). Ca^{2+} containing bath solution (25 μM) with a MTS reagent was prepared few minutes prior to application. All experiments were performed at room temperature (22°C).

Unless specified otherwise, Cys mutant channels were expressed in Xenopus Laevis oocytes. Frog care and handling procedures were in accordance with the *Comité de deontologie de l'experimentation sur les animaux* guidelines. Two years old X. Laevis frogs were anesthetized with 3-aminobenzoic acid ethyl ester, ovaries were surgically removed, and oocytes were dissected in Barth's solution containing the following:

90 mM NaCl, 1 mM KCl, 0.82 mM $MgSO_4$, 0.33 mM $Ca(NO_3)_2$, 0.41 mM $CaCl_2$, 5 mM HEPES (pH adjusted to 7.6 with NaOH). The follicular layer was removed by incubation in a Ca^{2+}-free Barth solution plus 1.75 mg/mL collagenase (SIGMA-Aldrich, Inc.) and 0.5 mg/mL trypsin inhibitor at room temperature for 60 min. The oocytes were then incubated in a Barth solution containing 1 mg/mL bovine serum albumin for 60 min to remove any remaining follicular cells.

Stage V and VI oocytes were stored at 18 °C in Barth's solution supplemented with 100 U/mL and 0.1 mg/mL streptomycin. Oocytes were studied 3-5 days after injection of the cDNA coding the mutant cystein K_{Ca}3.1 channels. Prior to the patch-clamp recordings, defolliculated oocytes were kept in hypertonic solution containing 250 mM KCl, 1 mM $MgSO_4$, 1 mM EGTA, 50mM sucrose and 10 mM HEPES buffered at pH 7.4 with KOH. The vitelline membrane was then peeled off using forceps, and the oocytes were transferred to a superfusion chamber for patch-clamp measurements.

2.2.1 Data Analysis

Channel activation and deactivation times were estimated from the variations of current following rapid addition (25 μM) or removal of $Ca^{2+}$from the internal medium before and after MTS application. Time constants of channel activation (τ_{on}) and deactivation (τ_{off}) were obtained by fitting to a single exponential of these time dependent changes on the Cys-MTS K_{Ca}3.1 currents. Possible structural changes resulting from MTS binding to the protein mutant channel were inferred from the change in open probability (P_o) measured at the single channel level.

Single channel kinetic parameters were estimated using the QuB software package (http://www.qub.buffalo.edu) from idealization of noisy recordings. This idealization procedure uses the segmental k-Means method based on Hidden Markov Modeling (HMM) (Qin, 2004). Several segments with time duration of 5 seconds were analyzed with this package.

To estimate the channel open probability (P_o), the current recorded was cosidered as being generated by a population of N identical channels, where the probability of the r channels are open over N ($P_N(r)$) is giving by:

$$P_N(r) = \frac{N!}{r!(N-r)!} P_o^r (1 - P_o)^{N-r} \tag{2.1}$$

Thus, the open probability of a single channel was thus computed from:

$$P_o = \frac{\sum P_N(r) r}{N} \tag{2.2}$$

Chapter 3

Results

3.1 Model structure of the Ca^{2+}/N-lobe/CaMBD2 complex

The graphic in figure 3.1a shows the value of the MODELLER objetive function (MOF) for the 100 structures generated by MODELLER. This objetive function is a quantitative parameter used for the ranking of the model structures which have the same sequence and spatial restraints based on the atomic distance in CHARMM (Brooks et al., 1983) parameters. The lowest 14 PDFs model values of the CAMBD region of the K_{Ca}3.1 were selected (red asterisks) and energy minimized using CHARMM force field (Brooks et al., 1983). These model structures were compared with the template by superposition of the C^{α} atoms. Best root mean square distance (RMSD) was used as criteria to select the final model structure of the CaMBD region of the Ca^{2+}/CaM/ K_{Ca}3.1 complexes(figure 3.1b). The best RMSD value was 1.83 Å. This value mainly reflects the difference in lenght of the the harpin region between the K_{Ca}3.1 and SK_{Ca}2.2 template CaMBD regions. The hairpin folding centered at R331 of the C-terminal region of the K_{Ca}3.1 is formed by only five residues compared to eight residues for SK_{Ca}2.2.

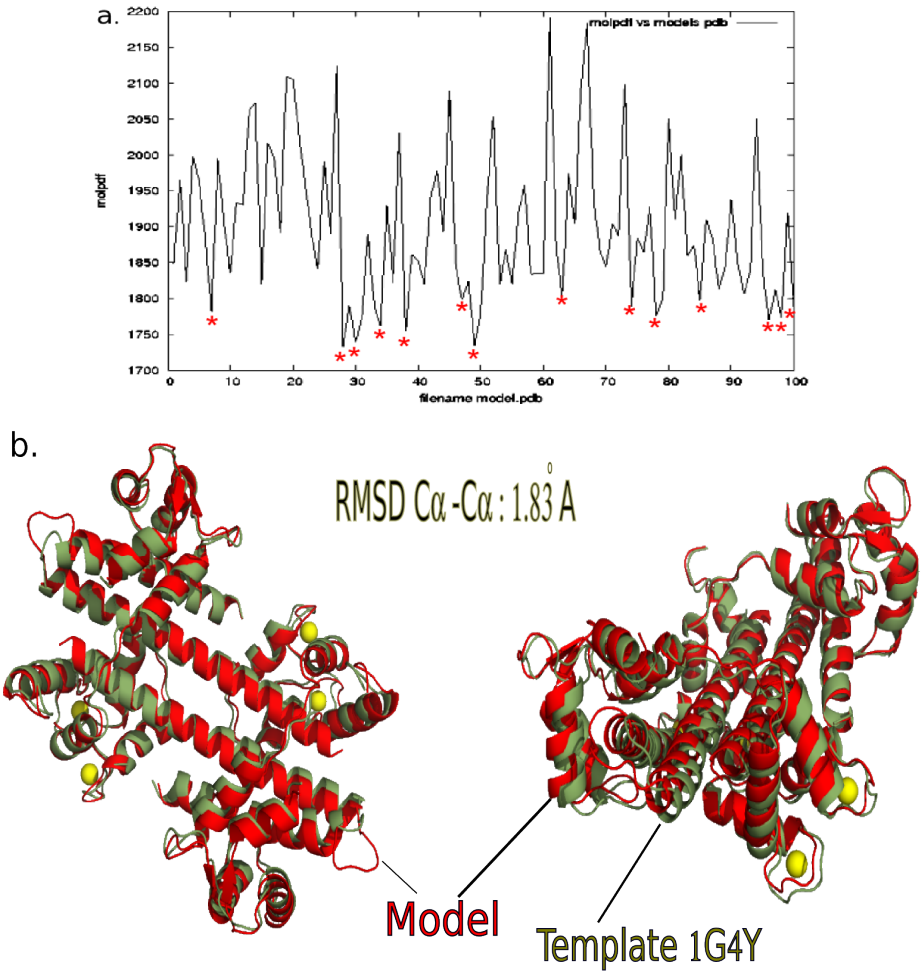

Figure 3.1: Graphics of the MODELLER objetive function (MOF) values of the 100 models structures. a. Asterisks in red show the 14 lowest pdf values of the 100 pdb structure models. b. Superposition between the best model structure (green) and template (red) structure (PDB:1G4Y).

Figure 3.2 shows a ribbon representation of the Ca^{2+}/CaM/KCa3.1 complex connected to the transmembrane S6 segments. The binding of $Ca^{2+}$to CaM (17kD) predicted to initiate a conformational change leading to the bringing of two adjacent K_{Ca}3.1 monomers in C-terminus at Calmodulin binding domain (CaMBD). The Calmodulin binding domain (CaMBD) at the C-terminus of K_{Ca}3.1 consists in a helical segment of 91 amino acids starting at the residue D304, with a hairpin folding 5 amino acid long centered at R331. The overall stoichiometry corresponds to one CaM molecule per monomer (figure 3.2a). The model presents a

first CaMBD domain (CAMBD1) located in segment 312-329 segment and a second domain (CAMBD2) extending from residues 361 to 372. The first domain is responsible for the constitutive Ca^{2+}-independent link to the CaM C-terminal lobe (C-lobe), whereas the second domain accounts for the Ca^{2+}/CaM N-terminal lobe (N-lobe) complex interaction (see figure 3.2b).

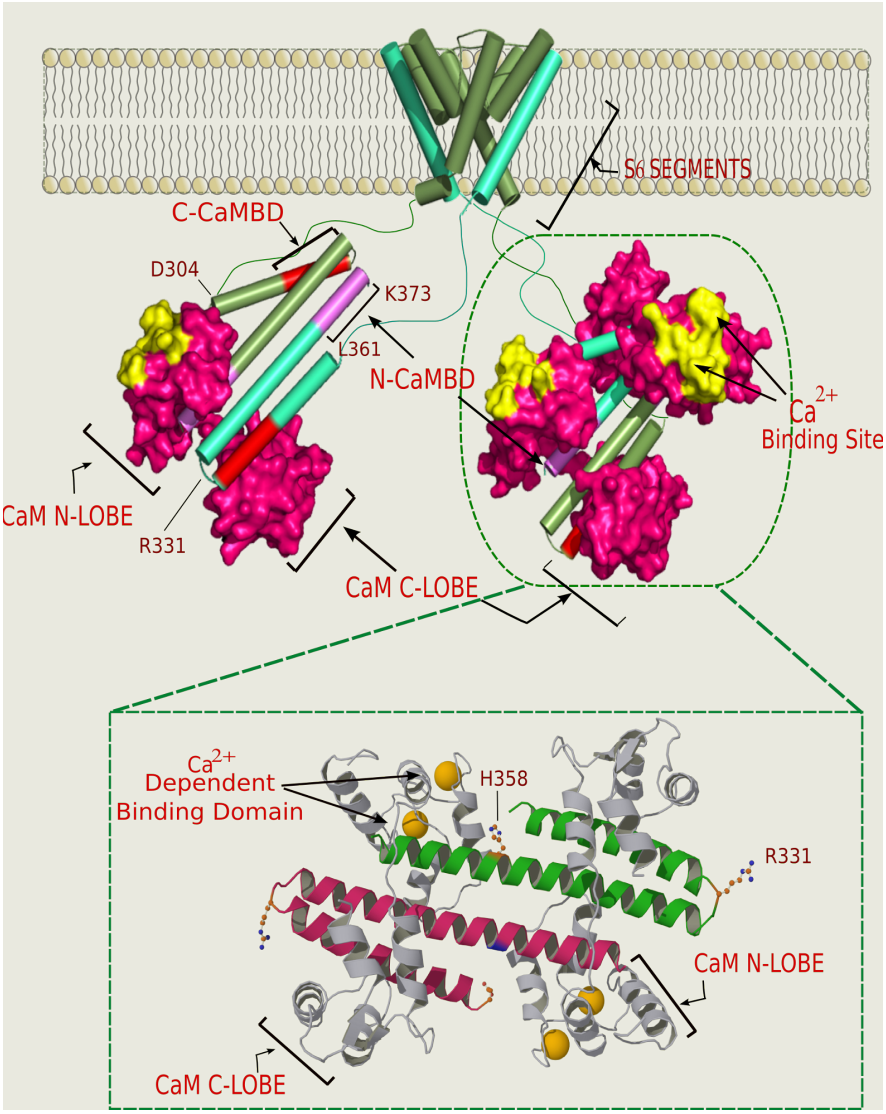

Figure 3.2: Cartoon representation of the CaM/K_{Ca}3.1 complex connected to the transmembrane S6 segments (a). Figure adapted from (Yellen, 2001). Ribbon representation of the Ca^{2+}/CaM/CaMBD complex (b) obtained by homology modeling using the solved crystal structure of the rat SK_{Ca}2.2 channel as template (PDB:1G4Y).

The model predicts that the KCa3.1 CaMBD2 residues L361, Q364, V365, M368 and I371 should be facing CaM with M368 buried in a hydrophobic pocket region of the CaM N-Lobe (helix A, B and D) and Q364 interacting with E45, E47, D50 and M51 in helix C of the N-lobe EF hand of CaM. In contrast, the E363 and N366 residues of KCa3.1 CaMBD2 should be projecting opposite to the CaM N-lobe (figure 3.3).

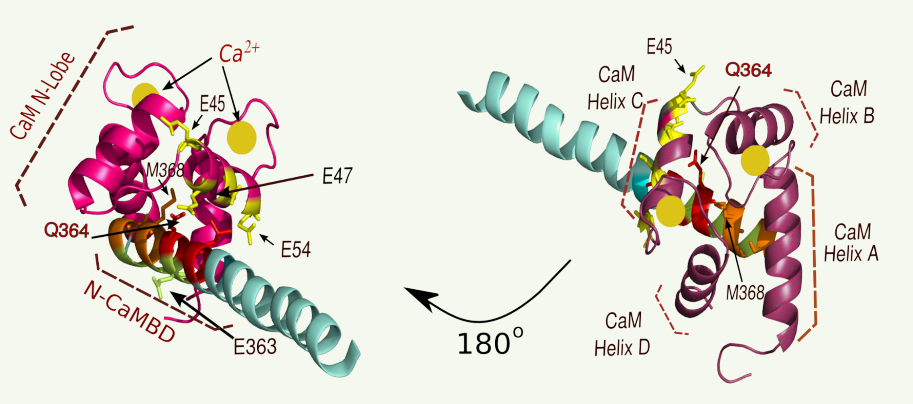

Figure 3.3: Side view of CaMBD2 region responsible for the Ca^{2+}-dependent binding to the CaM N-lobe. CaMBD2 is formed by residues extending from L361 to 372 (helix coloured of red, orange and green). Residue Q364 (red) of $K_{Ca}3.1$ is facing E45 and E47 (yellow coloured) of CaM whilst E363 is projecting opposite to the CaM N-lobe.

A more detailed description of the intermolecular protein-protein interactions between CaMBD2 region of the $K_{Ca}3.1$ channel and N-lobe of CaM was obtained using LIGPLOT software (Wallace et al., 1995). In this case, the CaMBD2 region was identified as the ligand protein (chain A) and CaM was the receptor (chain B) protein. Figure 3.4 shows the 2-D diagram representations of the intermolecular hydrogen bonds and hydrophobic interactions of the Ca^{2+}/CaMBD2/N-lobe complex. Atoms NZ and NE2 of L361 and Q364 are predicted to form hydrogen bonds with OE2 and OE1 atoms of E47 in the helix C of the CaM N-lobe. Hydrogen bond lengths for both electrostatic interactions were estimated at 3.00 Å.

The four other hydrogen bonds are predicted between N-lobe of CaM and the last residues of CaMBD2 region. Three hydrogen bond interactions were detected

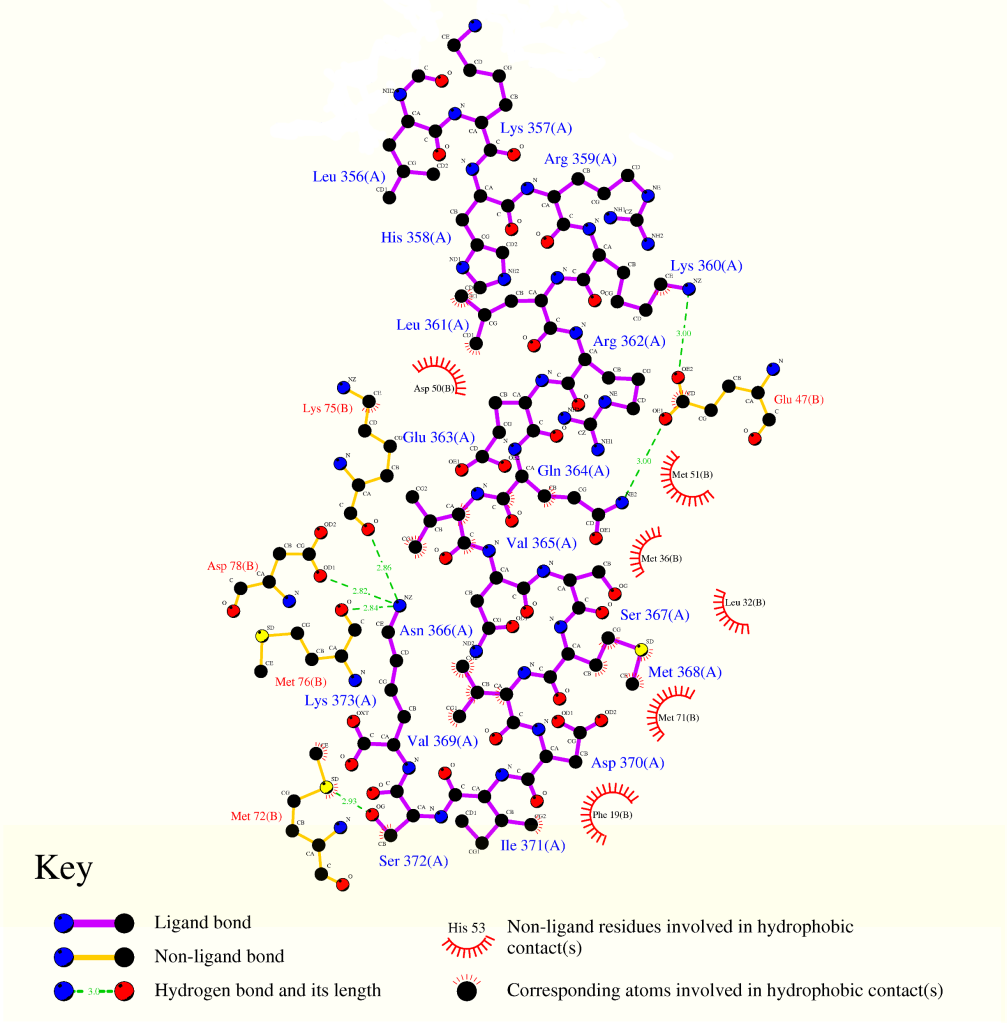

Figure 3.4: 2-D diagram representation of the intermolecular interactions between CaMBD2 and N-lobe of CaM. Protein-protein interactions were obtained using LIGPLOT software (Wallace et al., 1995).

between the NZ atom of K373 and atoms of the M76, D78 and K75 residues located in helix D of the CaM N-lobe (see fig 3.4). The forth hydrogen bond is predicted to take place between OG of S372 and SD atom of the CaM M72 residue. The lenght of hydrogen for these four intermolecular interactions was estimated at 2.82 Å, 2.84 Å, 2.86 Å and 2.93 Å respectively. Also, figure 3.4 shows important hydrophobic interactions between the CaM N-lobe and the $K_{Ca}3.1$ CaMBD2. Residues belonging to helices B (L32, and M36), C (M51) and D (M71 and M72) of the CaM N-lobe are seen to be involved in hydrophobic contacts with M368 and

V365 of CaMBD2. Cartoon and stick representations of the CaMBD2 and the N-lobe domain of CaM show that the M368 residue of CaMBD2 is located into the hydrophobic pocket formed for these hydrophobic residues (figure 3.4). Based on the Ca^{2+}/CaM/CaMBD2 complex model and calculations of intermolecular interactions, we hypothezed that the CaMBD2 segment of the $K_{Ca}3.1$ channel could be interacting with the Ca^{2+}saturated N-lobe domain of CaM by electrostatic interactions at the first K360-Q364 residues and through hydrophobic interactions at the S367-I371 region. The strong electrostatic interactions between the K372 residue of $K_{Ca}3.1$ and CaM residues could be more questionable as this residue is in the terminal region of the Ca^{2+}/CaM/$K_{Ca}3.1$ complex model and thus less likely to be properly modeled.

3.2 *SCAM* Analysis of the Ca^{2+}/N-lobe/CaMBD2 complex and MTS effects

To evaluate the proposed model of the Ca^{2+}/N-lobe/CaMBD2 $K_{Ca}3.1$ complex, we performed *SCAM* experiments using different methane thiosulfonate (MTS) reagents as described in material and methods. Figure 3.5 illustrates the effects of 1 mM of the positevely charged $MTSET^+$ and neutral MTSACE reagents on Cystein engineered at E363,Q364, V365 and S367 of $K_{Ca}3.1$.

Binding of $MTSET^+$ to R362 (data not shown), Q364C(fig 3.5c) or V365C (fig 3.5e) mutant channel caused an irreversible increase in channel activity. Such an effect was not seen for the Q364C mutant with application of 1mM the neutral MTSACE reagent (fig 3.5d), nor with $MTSET^+$ acting on E363 predicted be oriented opposite to the CaM N-lobe (fig 3.5a). These results are compatible with the model structure generated for Ca^{2+}/CaM/CaMBD2 complex, where the Q364 and V365 residues are facing E45, E47 and D50 of the CaM N-lobe. In contrast, $MTSET^+$ and

not MTSACE caused a clear current inhibition when reacting with S367C (fig 3.5g and 3.5h respectively), a residue predicted to be projecting inside the hydrophobic pocket of the CaM N-lobe.

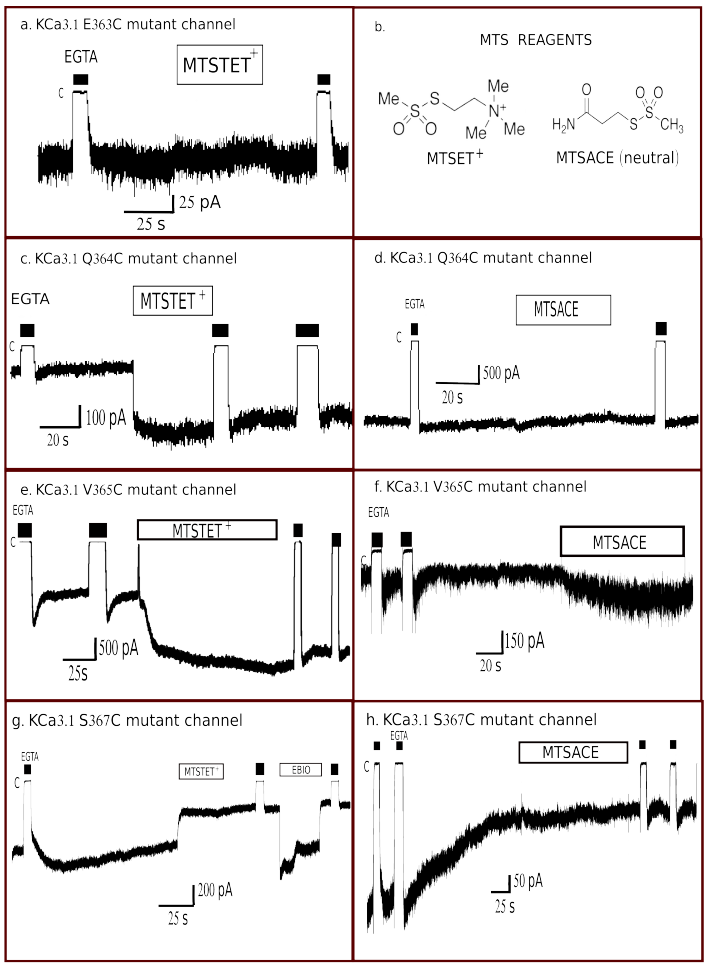

Figure 3.5: Inside out patch clamp recordings illustrating the action of 1mM $MTSET^+$ or 1mM MTSACE (neutraly charged) thiosulfonate reagents on the E363C, Q364C, V365C and S367C mutant channels. Current records were obtained at -60 mV in symmetrical 200 mM K_2SO_4 conditions with 25 μM of Ca^{2+}in the internal medium. Black rectangle identifies zero currents recorded when $Ca^{2+}$was removed (EGTA solution). Label C refers to the channel close configuration.

Quantification of the $MTSET^+$ effect on the current amplitude for $K_{Ca}3.1$ mutant channels from K360 to S372 is plotted in the figure 3.6. The bar graph represents in a logarithmic scale the ratio of the mean current of the mutant $K_{Ca}3.1$ channels in saturated Ca^{2+}concentration after (I_{MTSET}) and before (I_{ctrl}) 1 mM $MTSET^+$

application. Color code refers to an increase(red), absence(green) or inhibition (orange) in current caused by MTSET$^+$ acting on the Cys mutant.

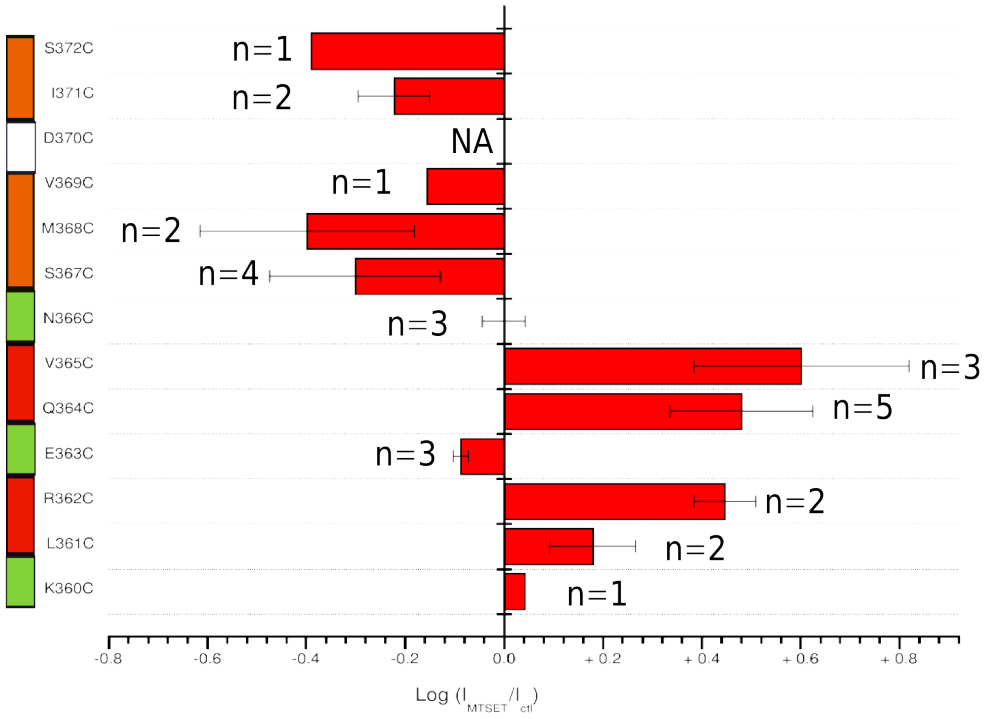

Figure 3.6: Effects of MTSET$^+$ on K_{Ca}3.1 mutant channels. Zero value indicates a total absence of MTSET$^+$ effects on channel activity. NA indicates no expression of D370C channel. Experiments were performed in 25 μM internal Ca^{2+}at pipette potential of -Vp = -60 mV.

The results obtained for the domain extending from K360-K372 show that the R362, Q364C and V365C mutant channels had their activity increased more than two folds after the covalent binding of the MTSET$^+$ (2.7 $\pm$ 0.6 ($n = 3$), 3 $\pm$1 ($n = 5$) and 4 $\pm$2 ($n = 3$) respectively), whereas a significative current inhibition was recorded for the S367C, M368C and I372C mutants with $< I_{MTSET} > / < I_{ctrl} >$ ratios of 0.5 $\pm$0.2 ($n = 4$), 0.4 $\pm$0.2 ($n = 2$) and 0.4 ($n = 1$) respectively. No observable effect was measured on the E363C and N366C mutant channel currents after MTSET$^+$ application, suggesting that these residues were not accessi-

ble to the hydrophilic $MTSET^+$ reagent or that the binding of $MTSET^+$ had no effect on the channel function. Second-order rate constants for the reaction of $MTSET^+$ were calculated for Q364C, V365C, S367C and M368C mutants as these channels presented a strong response to $MTSET^+$. The current variations were fitted to a single exponential. $MTSET^+$ modification rate for Q364C and V365C were $(11.2 \pm 5) X10^3 M^{-1} s^{-1}$ (n=4)) and $(5.5 \pm 1) X10^3 M^{-1} s^{-1}$ (n=2) indicating that these residues are free accessible to $MTSET^+$ whereas the modification rates for the S367C and M368C residues reflect an environment less favorable to the $MTSET^+$ binding ($(500 \pm 200) X10^3 M^{-1} s^{-1}$ and $(110 \pm 70) X10^3 M^{-1} s^{-1}$ respectively).

In addition, time constant of channel deactivation (τ_{off}) was extracted from the patch clamp recordings in order to analyze if the increase in mutant channel activity following $MTSET^+$ binding affects Ca^{2+}dependece. τ_{off} was obtained by fitting to a single exponential the time dependent decrease in current after Ca^{2+}removal from internal medium before and after $MTSET^+$ application for wild type (WT) and Cys channel mutations extending from K360 to M368.

The bar graph in figure 3.7 shows the ratio between the channel deactivation rate of the for cystein channel mutations (τ_{off}^{mut}) relative to wild type (τ_{off}^{wt}) before (green) and after (red) 1 mM $MTSET^+$ application. Binding of $MTSET^+$ to Q364C caused a significant increase ($p < 0.05$) in τ_{off} indicating a greater apparent Ca^{2+}affinity relative to wild type. An important increase in τ_{off}^{mut} was also observed on V365C (n=5) and S367C (n=2) mutants relative to WT but in contrast to the Q364C mutation, the resulting values were not an effect of the $MTSET^+$ application. The apparent increase on Ca^{2+}affinity of the R362C and Q364C mutation after $MTSET^+$ application is compatible with the increase in channel activity measured in SCAM current analysis.

As our experiments were performed at saturated Ca^{2+}conditons (25 μM), an increase of the current activity and a greater apparent Ca^{2+}affinity of the R362C

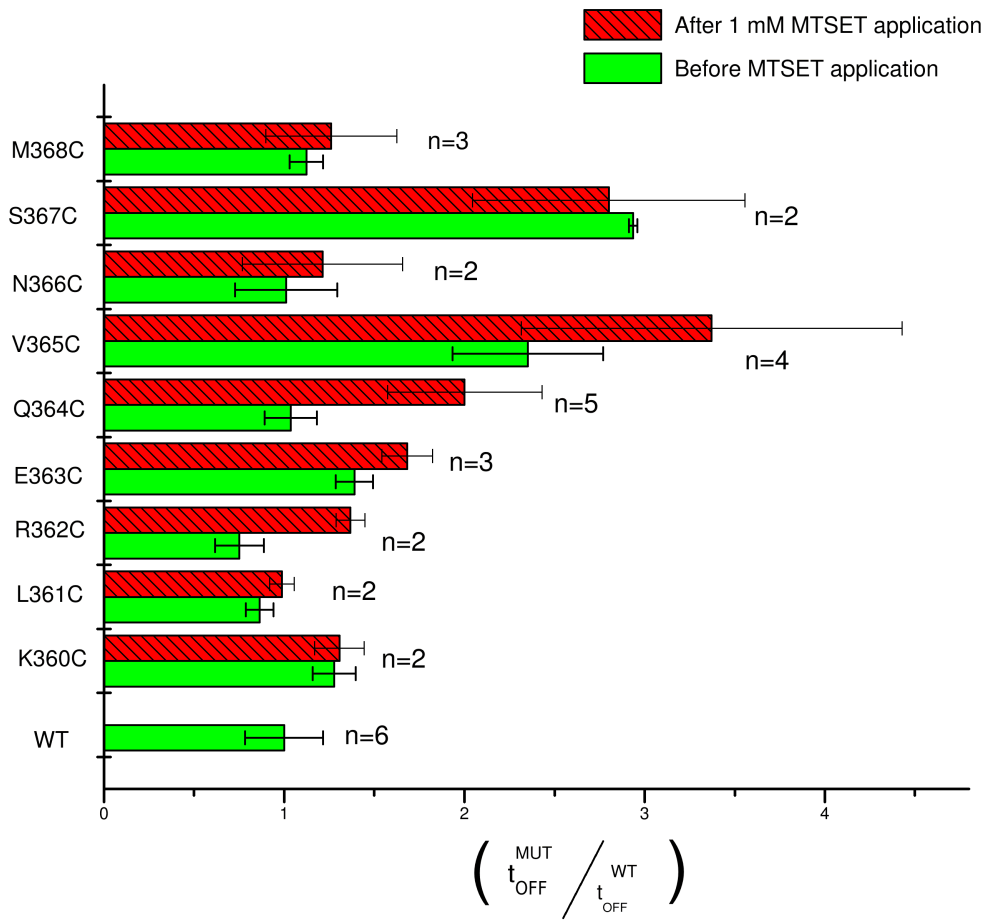

Figure 3.7: Bar graph of the time dependent deactivation rate (τ_{off}) before (green) and after 1 mM MTSET$^+$ application (red) for the wild type (WT) $K_{Ca}3.1$ channel and the cystein mutant channels at CaMBD2 region from K360 to 368 residues.

and Q364C mutant channels after MTSET$^+$ application, could be understood as a stabilization on electrostatic and/or steric interactions between the MTSET$^+$-Cys mutant channel and CaM N-lobe complex. Such a stabilization could arise from the covalent bound of MTSET$^+$ molecule to the 364C mutant thus increasing the interactions between Q364C and the negative residues E45, E47 and D50 at the helix C of the of CaM N-lobe (see fig 3.3). This residues are not implicated in the coordination binding of the Ca^{2+}ions at the Ca^{2+}loop regions of the binding sites (site I from 20 to 37 and site II from 56 to 67). Also a molecular dynamics simulation of the hydrophobic cleft in the N-domain of CaM loaded with Ca^{2+}ions

predicts that the effect of Ca^{2+} binding decreases the mobility of the Ca^{2+} loop regions and increases the helice motions with respect each other in order to provide the target binding by hydrophobic target recognition (Vigil et al., 2001). We thus performed inside-out recordings on the Q364C mutant channel using three different methanethiosulfonate reagents to test the nature of the interactions involved in the MTS effects. One of these MTS was $MTSES^{-}$ with dimemsions similar to $MTSET^{+}$ (5.8 Å X 6.4 Å X 8.9 Å) but bearing a negatively charge; $MTSEA^{+}$ and $MTSPtrEA^{+}$ are in contrast positively charged but have a volume different compared to $MTSET^{+}$ (Akabas et al., 1992) ($MTSEA^{+} < MTSET^{+} < MTSPtrEA^{+}$).

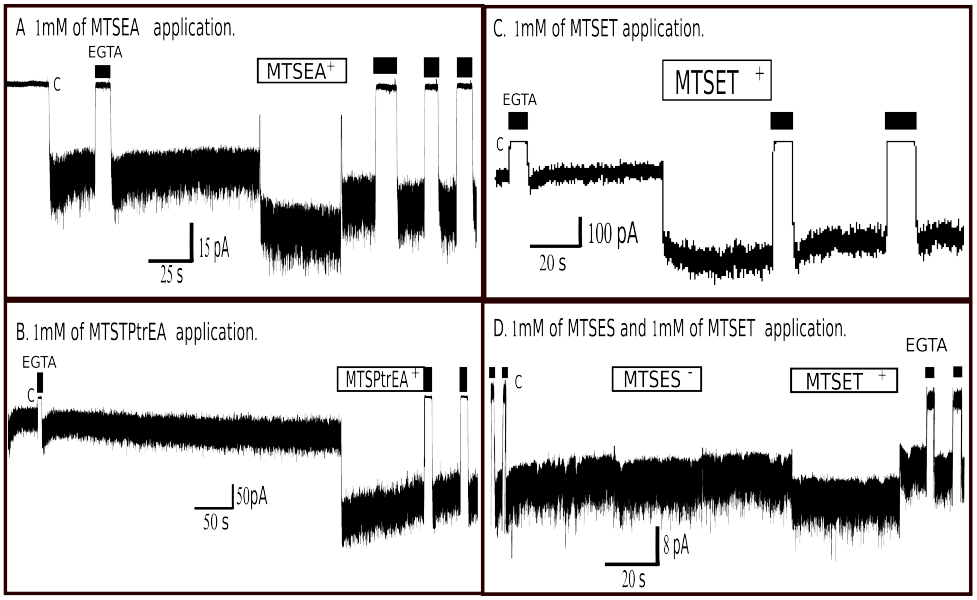

Figure 3.8: Inside out recordings illustrating the action of positively charged MTS reagents compared to the negatively charged MTSES(-) reagent on mutant Q364C channel. Current records were obtained at -60 mV in symmetrical 200 mM K_2SO_4 conditions with 25 μM of Ca^{2+}in the internal medium. Black rectangle identifies zero currents recorded when $Ca^{2+}$was removed (EGTA solution). Label C refers to the channel close configuration.

As seen in figure 3.8, an increase in Q364C mutant channel activity was observed with the positively charged reagents only $MTSEA^{+}$(A), $MTSPtrEA^{+}$(B), and $MTSET^{+}$(C) and not with $MTSES^{-}$ as described previously. Comparation of the amplitude of currents between the above mentioned MTS reagents and $MTSET^{+}$ (figure 3.8) suggests that the volume of the MTS reagents is not involved

in the stabilization interaction between the $K_{Ca}3.1$ Q364C mutant channel and CaM after MTS application. However their charge plays an important role in this interaction. Figure 3.8D provides more evidence of charge specific interactions of $MTSET^+$ reagent at position 364 as no effects was seen with $MTSES^-$.

3.3 Contribution of the CaM charge residues to the Ca^{2+}-dependent CaM/$K_{Ca}3.1$ interactions

To analyze the contribution of the CaM charge residues E45 and E47 to the formation of ionic bonds with Q364C-$MTSET^+$ complex, single and double mutant CaM E45A or E47A or E45A-E47A were generated and coexpressed with the Q364C mutant channel.

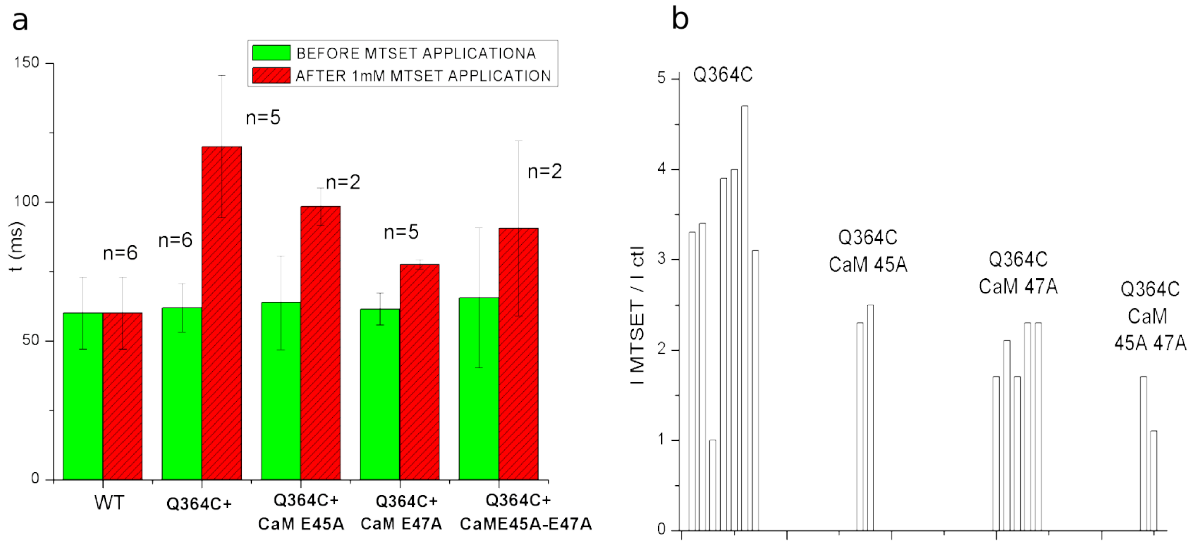

Figure 3.9: Neutralization effects of the CaM residues on electrostatic CaM/$K_{Ca}3.1$ interactions. A. Column graph illustrating how the neutralization of the E47 and/or E45 residues of the CaM N-lobe decreases the apparent Ca^{2+}affinity (faster (τ_{off})) of the Q364C mutant following binding of $MTSET^+$. B. Bar graph showing the effects of neutralizing E45 and/or E47 of the CaM helix C on the current increase induced by the binding of $MTSET^+$ onto the Q364C mutant. Each column represents a single experiment.

The results presented in figure 3.9a provide evidence for the role of the E47 residue in the stabilization of the CaM-Cys-MTSET$^+$ complex. Neutralization of the charge at E47 but not E45 significantly decreases ($p < 0.05$) the change in apparent Ca^{2+}affinity induced by MTSET$^+$ on the Q364C mutant with a τ_{off} for E47A-Q364C-MTSET$^+$ complex of $77 \pm 10ms$ (n=5) compared to $120 \pm 20ms$ (n=5) for the Q364C-MTSET$^+$ mutant channel. The ratios of the current after and before MTSET$^+$ application (I_{MTSET}/I_{ctrl}) for double (Q364C-E45A or Q364C-E47A) and triple (E45A-E47A-Q364C) mutant channels were measured and compared with the ratios of the Q364C mutant channel measured under the same conditions (figure 3.9b).

A decrease of the ratio I_{MTSET}/I_{ctrl} of the current in the triple mutant channel was found to be more more important than with the double mutants Q364C-E45A and Q364-E47A. These results strongly support a model where stabilizing the interactions between the CaM N-lobe and K_{Ca}3.1 CaMBD2 at Q364 through electrostatic interactions leads to an increase on channel activity at saturating Ca^{2+} concentrations.

3.4 Single channel analysis of MTSET$^+$ action on Q364C mutant

Inside-out single channel recordings of the Q364C mutant channel expressed in oocytes were carried out to understand at the single channel level the apparent increase in Ca^{2+}affinity of Q364C channel after internal application of 1 mM MTSET$^+$.

Figure 3.10 shows single channel current recordings of Q364C before (3.10a) and after 1 mM MTSET$^+$ application (3.10b). The label C refers to the zero current level. Estimation of the channel open probability (P_o) was obtained assuming

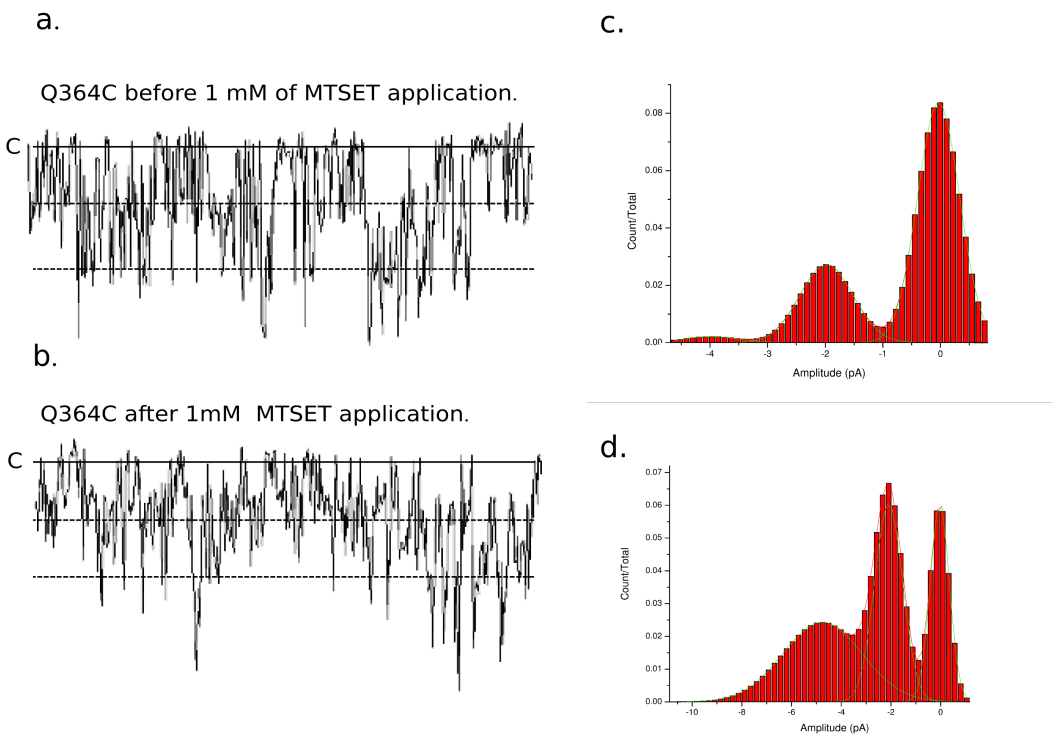

Figure 3.10: Single channel analysis of the MTSET$^+$ effect on Q364C mutant channel

a binomial distribution of N identical channels as described in the methodology section. As these inside-out patch clamp experiments were performed at saturating intracellular Ca^{2+}conditions (25 μM), P_o thus corresponds to ($P_{o_{max}}$).

The $P_{o_{max}}$ values were calculated from amplitude histograms showed in figures 3.10c and 3.10d. $P_{o_{max}}$ for the Q364C channel before MTSET$^+$ application was 0.29 and increased to 0.67 after 1 mM MTSET$^+$ application. The increase in $P_{o_{max}}$ was essentially arising from a decrease of the channel closed time, from 13 $\pm$ 4 ms to 4.5 $\pm$ 1 ms ($\backsim$ 1500 events) with no significative variation of the channel mean open time (from 7.60 $\pm$ 1.4 ms to 11.3 $\pm$ 2.6 ms before and after MTSET$^+$ application). These results provide an evidence of a destabilization of the closed configuration.

3.5 Implication of the Ca^{2+}/CaMBD2/CaM N-lobe interactions on Ca^{2+} dependent activation process

Recent experiments performed in our laboratory have shown that the mutation F248A in the selective filter caused an increase of the channel open probability due to a change in the open/closed energy balance of the channel gate at the selective filter. At the single channel level this variation is reflected on a increase of the mutant open probability (P_o = 0.66) at saturated Ca^{2+}concentration and a *burst* [1] kinetic behavior which allows to clearly distinguish the Ca^{2+}-dependent and Ca^{2+}-independent process on F248A mutant channel. In this *burst* fluctuation pattern, it was found that the *interburst* periods were Ca^{2+} dependent, where as channel gating within a *burst* was essentially Ca^{2+} independent. Experiments were performed with a double mutant F248A-Q364C to determine how the effect of $MTSET^+$ on the Ca^{2+}/CaMBD2/CaM N-lobe interactions affects the Ca^{2+}dependent activation process.

Figure 3.11. illustrates the single channel currents of the double mutant Q364C-F248A, which were produced at Ca^{2+}concentrations of 0.4 μM, 0.6 μM and 25 μM. Kinetic properties the *burst* behavior were clearly observed at 0.4 μM Ca^{2+}concentration. Two closed time periods were identified whilst only one burst of openings was detected. Increasing Ca^{2+}concentration at 0.6 μM produced a notable reduction the longer closed time periods *interburst* in Q364C-F248A single current. At saturated Ca^{2+}concentrations the *interburst* segments were hardly distinguished from the closed dwell time value of P_o within the *burst* does not change. These observations demostrate that in single Q364C-F248A recordings the Ca^{2+}-dependent process is associated to the interburst periods. The mutant channel $P_{o_{max}}$ at saturated concentrations was 0.55 . This value is similar to the $P_{o_{max}}$ value obtained for

[1] The *burst* term is used after the work of Colquhoun and Sakmann (Colquhoun and Sakmann, 1983)

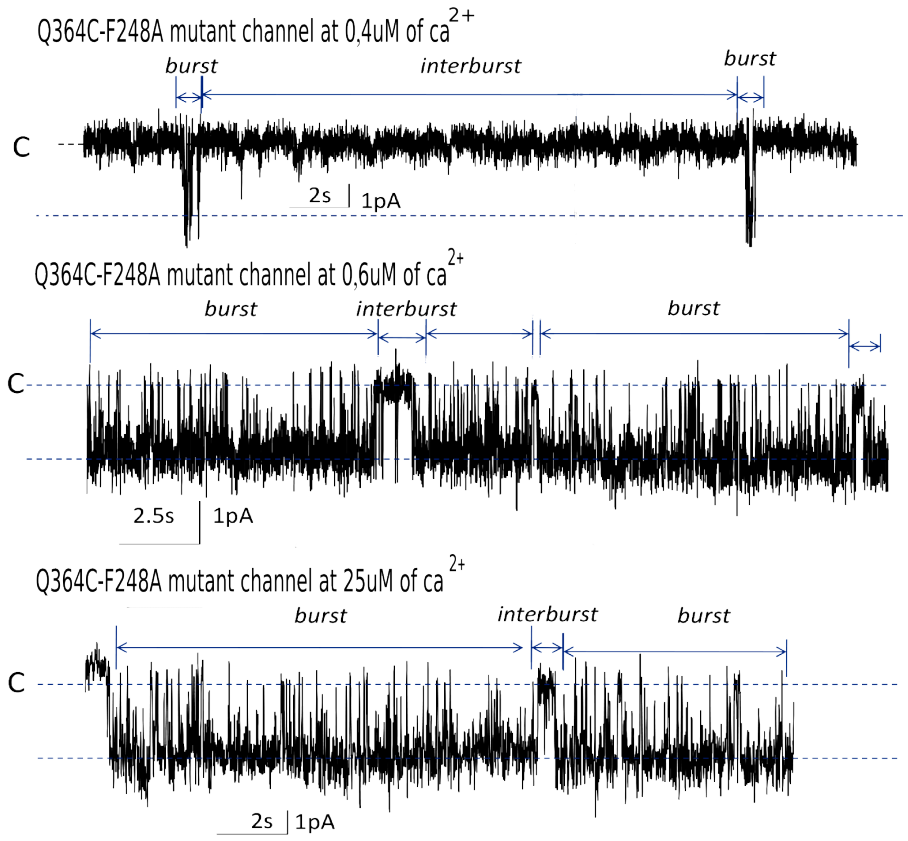

Figure 3.11: Single channel recordings of the mutant Q364C-F248A at three different Ca^{2+}concentrations. Single channel currents present a *kinetic burst* behavior with a long closed state *interburst* which separate a group of openings with short closed state *burst*. Increase on Ca^{2+}concentration produces, in single channel current a reduction of the long closed state.

the single current of the mutant Q364C channel after 1 mM of $MTSET^{+}$ application (see section 3.4). Therefore, we hypothesized that the double mutant Q364C-F248A channel current would not be affected by $MTSET^{+}$ at saturating Ca^{2+}.

The figure 3.12 shows the macroscopic current elicited by Q364C-F248A mutant channels. Figure 3.12A illustrates the current amplitudes of the Q364C-F248A channel at saturated Ca^{2+} concentration with and without $MTSET^{+}$ application. As expected, no effect of $MTSET^{+}$ binding was observed at saturated Ca^{2+} concentration for this double mutant channel. Also current activity of this mutant was recorded at different Ca^{2+}concentrations (figure 3.12B) and plotted as a Ca^{2+} dose-response curve.

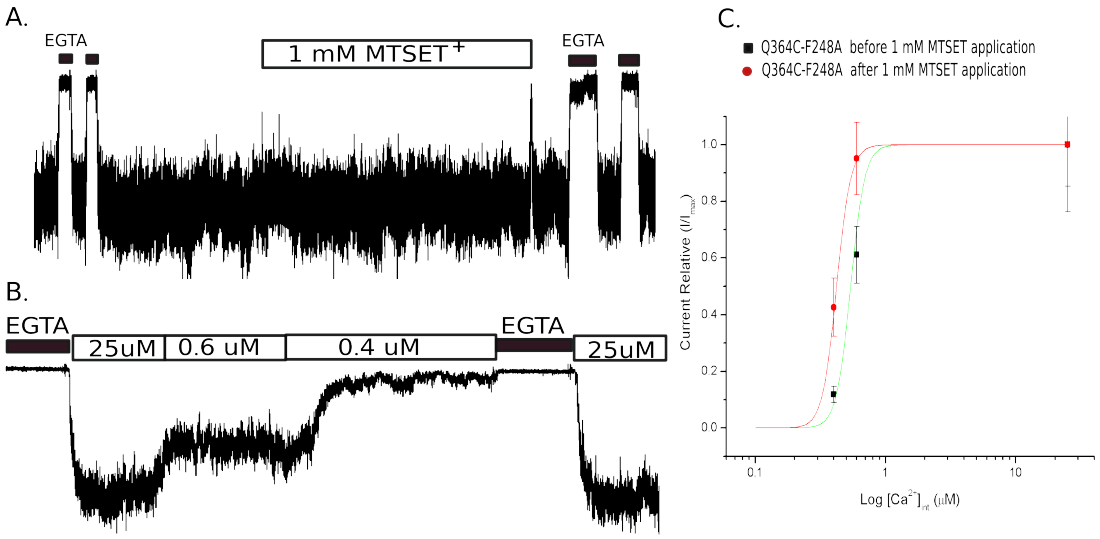

Figure 3.12: F248A-Q364C mutant channel behavior. Figure 3.12A shows patch current traces recorded from the Q364C-F248A channel at saturated Ca^{2+} concentration with and without $MTSET^{+}$ application. Figure 3.12B illustrates the sensivity of the mutant F248A-Q364C current to the variation of Ca^{2+} concentrations. Figure 3.12C Ca^{2+}dose-response curve of F248A-Q364C in the presence or absence of 1 mM of $MTSET^{+}$.

Figure 3.12C presents the Ca^{2+}dose-response curve obtained for F248A-Q364C mutant from patch clamp protocol in the presence or absence of 1 mM of $MTSET^{+}$. Current levels at -60 mV were normalized from the maximal current amplitude obtained at 25μM of Ca^{2+}. Each Ca^{2+}dose-reponse curve was fitted to a Hill equation. The Ca^{2+}dose-reponse curve in absence of 1 mM of $MTSET^{+}$ shows that Ca^{2+}activates mutant channel with an EC_{50} of 0.5 μM and a Hill coefficient of 8. In constrast, in presence of 1 mM of $MTSET^{+}$, the EC_{50} value was 0.4 μM with an equal Hill coefficient of 8. This last result is in accordance with the increase of the apparent Ca^{2+}affinity reflected on the increase of the deactivation time constant for Q364C mutant channel (see section 3.2). In addition the effect of $MTSET^{+}$ binding to Q364C-F248A mutation on channel activity was not observed at saturating Ca^{2+} concentration indicating that the channel activity in this condition was already maximal.

Chapter 4

Discussion

The mechanism by which the binding of Ca^{2+}ions to the CaM/K_{Ca}3.1 complex would lead to the opening of a gate located at the level of the selectivity filter is not currently known. The use of comparative modeling methods and key experimental techniques provided clues on structure and function properties of the K_{Ca}3.1 CaMBD2 complexed with the Ca^{2+}-dependent domain of CaM that would lead to interactions susceptible to affect the channel gate.

4.1 Characterization of the CaM binding domain motif CaMBD2

The homology model obtained for the Ca^{2+}/CaM/K_{Ca}3.1 structure displays a great analogy with the Ca^{2+}/CaM/SK_{Ca}2.2 3D structure (RMSD=1.83Å), proving that the X-ray structure of the Ca^{2+}/CaM/SK_{Ca}2.2 complex is a convenient template to model the structure of the CaM binding domains of K_{Ca}3.1 with CaM in the presence of Ca^{2+}ions. A structural analysis of the interactions between Ca^{2+}-dependent N-lobe and the CaMBD2 of K_{Ca}3.1 allowed to characterize two segments in this domain which interact differently with the N-lobe domain of CaM.

The first segment extending from K360 to Q365 displaied hydrophilic characteristisc which allow to interact electrostatically with the helix C of CaM N-lobe. In contrast, the second segment from S367 to I371 presented hydrophobic properties which would favour hydrophobic interactions with a lot of hydrophobic CaM residues particularly with Methione residues.

Our *SCAM* analysis using $MTSET^+$ reagent (see section 3.2) provided strong evidence showing that Cys engineered at positions in the 361-365 segment facing to the CaM N-lobe complexed with $MTSET^+$ stabilize the CAM-Cys-mutant-$MTSET^+$ channel activity by electrostatic interactions. An inhibitory effect was in contrast observed with the Cys mutant channels at the second segment of the CaMBD2 (366-372) when $MTSET^+$ was applied. These results are in agreement with the consensus features of the CaM binding target sequences, which are characterized by the relevant role of both the basic and hydrophobic residues on the CaM recruitment signaling (CRS) motifs (O'Neil and DeGrado, 1990; Yap et al., 2000).

Positions of the $K_{Ca}3.1$ hydrophobic residues L361, V365 and M368 and basic residues R359, K360 and K373 obtained from the model structure allow to propose a possible alignment with the CaM peptide target sequences belonging to the 1-5-8-14 subclass of the CRS motifs (the numbers indicate the key position of the hydrophobic residues on the CaM's targets recognition).

CaMBD sequence of the $SK_{Ca}2.2$ channel contains no identifiable CaM interactions motif, in contrast, as seen in figure 4.1, the sequence of the CaMBD2 $K_{Ca}3.1$ motif can be clearly associated with the well known CaM target binding domains of the rat olfatory cyclic nucleotide-gated channel (*OCNC*) (Liu et al., 1994), the $G_{\beta\gamma}$ subunit (Liu et al., 1997), the Calcineurin subunit A (Kincaid et al., 1988) and the Murin-inducible nitric oxide synthase (Murin i*NOS*) segment from 501 to 532 (Venema et al., 1996). The CaMBD2 sequence of the $SK_{Ca}2.2$ lacks the last

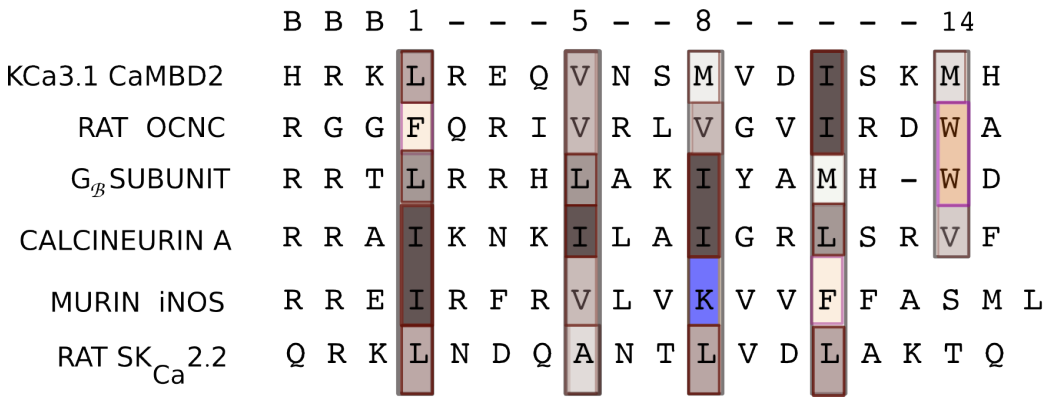

Figure 4.1: Alignment of the CaM binding target sequences of the rat olfatory cyclic nucleotide-gated channel, the $G_{\beta\gamma}$ subunit, the Calcineurin A subunit and the Murin-inducible nitric oxide synthase, which are members of the 1-5-8-14 subclass CRS motifs. Grey colos scale identifies the hydrophobic residues of the CRS members motif, pink color distinguishes the aromatic residues and blue color the basic residues.

key hydrophobic residue 14 to complete the 1-5-8-14 CaM target motif (see figure 4.1). The absence of this residue and the unusual tridimensional structure of the Ca^{2+}/CaM/SK_{Ca}2.2 complex did not allow to associate at this time the CaMBDs of the SK_{Ca}2.2 to a consensus CRS motif.

Comparision between both CaM binding domain sequences of the Calcineurin subunit A and KCa3.1 channel was performed using an hydrophobic cluster analysis (*HCA*) (Gaboriaud et al., 1987). Figure 4.2 shows the CaMBD α helix 2D representation of the hydrophobic cluster patterns for the Calcineurin subunit A (left) and the CaMBD2 of K_{Ca}3.1 (right). In both diagrams the hydrophobic clusters were delimited by a red solid line. The gray scale refers to the hydrophobic residues involved in defining a CaM pattern target sequence, blue circles represent the basic amino acids near a hydrophobic cluster which can be involved in CaM pattern recognition. 2D patterns between both CaMBD sequeces show that residues L361, V365, M368 and I371 of K_{Ca}3.1 match as anchor hydrophobic residues susceptible interact with CaM protein similar to Calcineurin subunit A protein. $MTSET^{+}$ binding effects on the current of these mutant channels and intermolecular interactions calculations support the crucial interactions between these residues and CaM

protein. Interestingly, residues R362 and Q364 on CaMBD2 of the $K_{Ca}3.1$ (yellow circles) are located at the same position that two lysine residues (yellow circles too) which are near the hydrophobic match residues on Calcineurin protein.

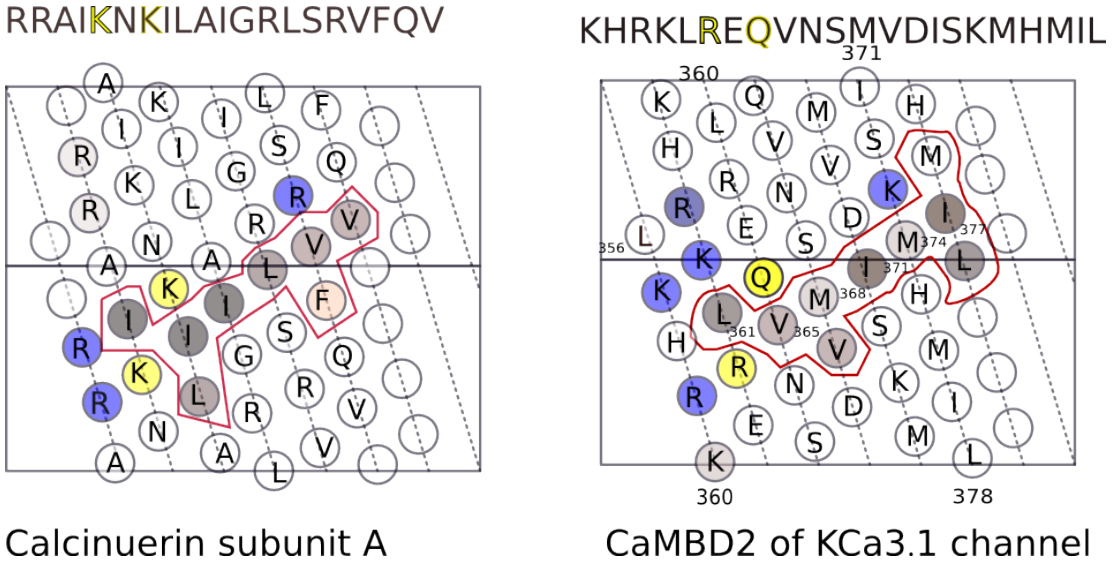

Figure 4.2: 2D pattern representations of the CaM binding domains of Calcineurin subunit A (left) and CaMBD2 of the $K_{Ca}3.1$ (right) by Hydrophobic cluster analysis.

Currently, there is a large number of 3D structures of proteins interacting with CaM protein in different ways (Hoeflich and Ikura, 2002; Yap et al., 2003), thus enabling a comparison of their structural features with our template structure. It is the case of the Petunia glutamate decarboxylase (Petunia *GAD*) 3D structure (PDB:1NWD) which interacts with CaM by two identical antiparallel CaM binding domains. This interaction forms a dimeric complex similar to the CaM/$SK_{Ca}2.2$ complex, but, the interhelical angle and direction of these interactions are different (Yap et al., 2003). Superposition of the CaMBD of the Petunia GAD interacting with CaM N-lobe domain and Ca^{2+}/CaM$SK_{Ca}2.2$ complex, revealed a close 3D identity between both complexes (RMS = 2.15) . Visual inspection of the Petunia GAD/CaM complex showed hydrophobic residues M14, W18 and F21 located at the same positions than L361, V365, M368 residues on the Ca^{2+}/CaM/$K_{Ca}3.1$ complex. All these results strongly indicate that the CaMBD2 of the $K_{Ca}3.1$ with

the hydrophobic residues L361, V365, M368 and M374 are implied on CaM target recognition.

The structural information of the $SK_{Ca}2.2$ crystal showed that Q476 interacts with residues belonging to the loop of the CaM N-lobe M36, Q41, P43 and only interacts with the E47 residue located at the helix C of CaM N-lobe. Also, residue L480 on $SK_{Ca}2.2$ displays a large number of contacts than M368 of the $K_{Ca}3.1$ with methionine and hydrophobic residues (M36, M51, M71, F19, L32 and F68) at the hydrophobic pocket of the CaM N-lobe (supplementary information (Schumacher et al., 2001)). CaMBD2 segment of the $SK_{Ca}2.2$ and $K_{Ca}3.1$ channels have a highly homology (see figure 2.1) but $SK_{Ca}2.2$ displays a greater $P_{o_{max}}$ compared to $K_{Ca}3.1$.

To determine if these features would be an effect of the different residues between $SK_{Ca}2.2$ and $K_{Ca}3.1$ in CaMBD2 complementary experiments should be carried on the wild type $K_{Ca}3.1$ channel where residues that differ from $SK_{Ca}2.2$ will be replaced by their $SK_{Ca}2.2$ equivalent (R362N, V365A, S367T and M368L) and the channel mutant activity measured in patch clamp experiments.

4.2 Stabilization of $K_{Ca}3.1$ channel for CaM N-lobe and CaMBD2 interactions

Our observation of a decreased mean close time following modification of the Q364C channel by $MTSET^+$, provides support for a simple kinetic model that accounts the increase in P_o value induced by $MTSET^+$. The following kinetic scheme accounts for the bursting pattern of $K_{Ca}3.1$ with two non conducting configurations and a single conducting state.

The first non conductive state C_0 represents the channel in the absence of calcium, while the closed state C corresponds to interburst state with Ca^{2+} ions bound to the CaM N-lobe binding sites, allowing the channel bursting from the trasitions

C to O states and vice versa. In the scheme 4.1, k_r refers to the Ca^{2+} dependent transition rate between C_0 and C states while k_i is the Ca^{2+} independent transition rate between C and C_0 states. α and β are the transition rates between the channel open conducting state and the channel closed state C.

$$C_0 \underset{k_i}{\overset{k_r\,[Ca^{2+}]}{\rightleftarrows}} C \underset{\beta}{\overset{\alpha}{\rightleftarrows}} O$$

Figure 4.3: Basic Kinetic model for a monomer structure of the $K_{Ca}3.1$ channel.

This model can account for the appearance of burst with:

$$\tau_{burst} = \frac{1}{k_i}\left(\frac{\alpha+\beta}{\beta}\right) \quad and \quad \tau_{interburst} \cong \frac{1}{k_r[Ca^{2+}]} \tag{4.1}$$

And P_o can be expressed as:

$$P_o = \frac{\alpha k_r[Ca^{2+}]}{\alpha k_r[Ca^{2+}] + \beta(k_r[Ca^{2+}] + k_i)} \tag{4.2}$$

According to this equation, an increasing P_o by MTSET$^+$ acting an Q364C can be caused by a decrease of either k_i/k_r or β/α or both. A decrease in β corresponds to an increase of the mean open time. Because this was not detectable in the single channel analysis of MTSET$^+$-Q364C complex (section 3.4), β value has been assumed to be constant, suggesting that a decrease in k_i/k_r factor and/or an increase in α value might explain the increase of $P_{o_{max}}$.

In addition results obtained with the double mutant Q364C-F248A results (section 3.5) provided evidence for a role the Ca^{2+}/CaMBD2/CaM interactions on the Ca^{2+} dependent activation process. Stabilization of Ca^{2+}/CaMBD2/N-lobe complex by electrostatic interactions shifts towards the left the Ca^{2+}dose-response curve, in accordance with increase of apparent Ca^{2+} affinity observated on τ_{off}

parameter. Single channel recordings provided also evidence for a stabilization of the complex with $MTSET^+$ coming from a decrease of the k_i/k_r energy balance which was reflected on a reduction of the interburst periods.

Therefore, the increase of $P_{o_{max}}$ by stabilization of the Ca^{2+}/CaMBD2/N-lobe complex at saturated Ca^{2+}concentration can be interpreted in the light of a better coupling of the Ca^{2+}/CaM/K_{Ca}3.1 conformatinal change induced by Ca^{2+} to the CaM C-lobe EF hand, which is constitutively bound to the proximal C-terminal region of K_{Ca}3.1 leading to a new conformational arrangement of the hydrophobic residues of S6 that will destabilize the closed states by interacting with residues of the selectivity filter.

Phosphorylation of residue H358 in the C-terminus by action of the NDPK-B increases three folds the channel currents (Gerlach et al., 2001; Srivastava et al., 2006). This modulatory process in the context of our model could be associated to a perturbation of the Ca^{2+}/N-lobe/CaMBD2 complex interactions which increase the $P_{o_{max}}$. It has also been documented that the binding of the some openers such as 1-EBIO (Walker et al., 2001; Pedarzani et al., 2001) and CyPPA (Hougaard et al., 2008) are mediated via C-teminus interactions of the SK_{Ca} channels. We hypotesize that these effects could be modulated by the CaM/K_{Ca}3.1(L361-M374) interactions.

Our work reveals a new role of the cytoplasmic CaM N-lobe domain associated to CaMBD2 on K_{Ca}3.1 channel activity in mediating Ca^{2+}stimuli response. A recent study based on mutations of the N-lobe of CaM on SK_{Ca}2.2 showed that the N-lobe can affect the constitutive association between CaM and SK channel subunits (Li et al., 2009). This evidence supports our results relative to the crucial role of the interactions between the second domain of K_{Ca}3.1 channel and the Ca^{2+}-dependent domain of CaM on the channel regulation.

Chapter 5

Conclusions

Our results indicate a dominant electrostatic interaction between the Cys-MTSET$^+$ complex at position 364 and residues E45 and E47 of the CaM N-lobe. Increasing this interaction by covalent binding of MTSET$^+$ to a Cys at Q364C resulted in an increased channel activity at saturating Ca^{2+} concentration (25μM). This observation indicates that the channel maximum open probability $P_{o_{max}}$ is not only governed by interactions at the level of the gate (selectivity filter), but also by the strength of the coupling between the CaM and the K_{Ca}3.1 N-CaMBD.

Our SCAM analysis argues for a K_{Ca}3.1 Ca^{2+}-dependent CaMBD with two distinct regions: A first domain (K360-N366) where the stabilization of CaM/KCa3.1 complex involves interactions with the hydrophilic residues of the CaM N-lobe located on helix C, and a second domain where stabilization of the CaM/KCa3.1 complex arises from hydrophobic interactions in which residues of KCa3.1 (S367-M368) are projecting inside a hydrophobic pocket formed by helices A,B and D of the CaM N-lobe.

The phosphorylation of H358 in C-terminus by NDPK-B has been documented to cause an increase in the K_{Ca}3.1 channel activity. This effect requires the presence of Ca^{2+} and has been seen at saturating Ca^{2+} concentrations (increased $P_{o_{max}}$). The

homology based model of the CaM/KCa3.1 complex, presented locates H358 in proximity of the E54 residue of the CaM-N lobe, suggesting a possible rearrangement of the E45-E54 segment of CaM relative to the L361-V365 region of KCa3.1, and thus a possible change in the interaction CaM/KCa3.1.

The study performed in the present work provides new and initial information about how first signal transduction based on ligand binding and protein-protein interactions contribute to the channel gating properties of the Ca^{2+}-activated K^{+} channels. Currently, new studies on CaM/K_{Ca}3.1 interactions using different Q364 mutations are being conducted in our laboratory in order to understand how gating dynamics is occuring at the molecular level.

Further research using molecular simulations and site-direct mutagenesis could provide more information about the free energy contribution of the CaMBD2 residues to the channel stabilization. In addition, this dimer model has allowed to generate a heterotetramer dimer-dimer structure of the CaM/K_{Ca}3.1 complex by docking methods, which will enabling to learn more about such gating channel mechanisms and protein-protein interactions. Altogether these data should provide a better understanding of the relationship between structure and function among Ca^{2+}-activated K^{+} channels.

Bibliography

Akabas, M., D. Stauffer, M. Xu, and A. Karlin (1992). Acetylcholine receptor channel structure probed in cysteine-substitution mutants. *Science 258*(5080), 307.

Brooks, B., R. Bruccoleri, B. Olafson, et al. (1983). CHARMM: A program for macromolecular energy, minimization, and dynamics calculations. *Journal of computational chemistry 4*(2), 187–217.

Bruening-Wright, A., W. Lee, J. Adelman, and J. Maylie (2007). Evidence for a Deep Pore Activation Gate in Small Conductance Ca2+-activated K+ Channels. *Journal of General Physiology 130*(6), 601.

Chandy, K., H. Wulff, C. Beeton, M. Pennington, G. Gutman, and M. Cahalan (2004). K+ channels as targets for specific immunomodulation. *Trends in pharmacological sciences 25*(5), 280–289.

Chris, B., T. J. Maylie, and J. P. Adelman (1998). Small-conductance calcium-activated potassium channels. *Annals New York Academy of sciences*, 370–378.

Colquhoun, D. and B. Sakmann (1983). Bursts of openings in transmitter-activated ion channels. *Single-channel recording*, 345–363.

Cruse, G., S. Duffy, C. Brightling, and P. Bradding (2006). Functional KCa3. 1 K+ channels are required for human lung mast cell migration. *Thorax 61*(10), 880.

Devor, D., A. Singh, R. Frizzell, and R. Bridges (1996). Modulation of Cl-secretion by benzimidazolones. I. Direct activation of a Ca (2+)-dependent K+ channel. *American Journal of Physiology- Lung Cellular and Molecular Physiology 271*(5), 775.

Doyle, D., J. Cabral, R. Pfuetzner, A. Kuo, J. Gulbis, S. Cohen, B. Chait, and R. MacKinnon (1998). The structure of the potassium channel: molecular basis of K+ conduction and selectivity. *science 280*(5360), 69.

Doyle, M. and J. Egan (2003). Pharmacological agents that directly modulate insulin secretion. *Pharmacological reviews 55*(1), 105.

Edwards, G. and A. Weston (2004). Potassium and potassium clouds in endothelium-dependent hyperpolarizations. *Pharmacological research 49*(6), 535–541.

Eisenman, G., R. Latorre, and C. Miller (1986). Multi-ion conduction and selectivity in the high-conductance Ca++-activated K+ channel from skeletal muscle. *Biophysical journal 50*(6), 1025–1034.

et al, R. (1963). Stereochemistry of polypeptide chain configurations. *J. Mol. Biol. 7*, 95–99.

Félétou, M. and P. Vanhoutte (2007). Endothelium-dependent hyperpolarizations: Past beliefs and present facts. *Annals of medicine 39*(7), 495–516.

Gaboriaud, C., V. Bissery, T. Benchetrit, and J. Mornon (1987). Hydrophobic cluster analysis: an efficient new way to compare and analyse amino acid sequences. *FEBS letters 224*(1), 149–155.

Gao, L., J. Yankaskas, C. Fuller, E. Sorscher, S. Matalon, H. Forman, and C. Venglarik (2001). Chlorzoxazone or 1-EBIO increases Na+ absorption across

cystic fibrosis airway epithelial cells. *American Journal of Physiology- Lung Cellular and Molecular Physiology 281*(5), 1123.

Gardos, G. (1958). The function of calcium in the potassium permeability of human erythrocytes. *Biochimica et Biophysica Acta 30*, 653–654.

Garneau, L., H. Klein, U. Banderali, A. Longpré-Lauzon, L. Parent, and R. Sauvé (2009). Hydrophobic Interactions as Key Determinants to the KCa3. 1 Channel Closed Configuration. *Journal of Biological Chemistry 284*(1), 389.

Gerlach, A., N. Gangopadhyay, and D. Devor (2000). Kinase-dependent regulation of the intermediate conductance, calcium-dependent potassium channel, hIK1. *Journal of Biological Chemistry 275*(1), 585.

Gerlach, A., C. Syme, L. Giltinan, A. J.P, and D. Devor (2001). ATP-dependent activation of the intermediate conductance Ca2+-activated K+ channel hIK1 is conferred by a C-terminal domain. *Journal of Biological Chemistry 276*(14), 10963.

Griffith, T. (2004). Endothelium-dependent smooth muscle hyperpolarization: do gap junctions provide a unifying hypothesis? *British journal of pharmacology 141*(6), 881.

Hamill, O., A. Marty, E. Neher, B. Sakmann, and F. Sigworth (1981). Improved patch-clamp techniques for high-resolution current recording from cells and cell-free membrane patches. *Pflugers Archiv : European journal of physiology 391*, 85–100.

Heginbotham, L., T. Abramson, and R. MacKinnon (1992). A functional connection between the pores of distantly related ion channels as revealed by mutant K+ channels. *Science 258*(5085), 1152–1155.

Hesse, W., E. Moller, M. Arnold, and B. Schack (2003). The use of time-variant EEG Granger causality for inspecting directed interdependencies of neural assemblies. *Journal of Neuroscience Methods 124*(1), 27–44.

Hille, B. (2001). *Ion Channels of Excitable Membranes* (3 edition ed.). Sinauer Associates.

Hodgkin, A. and R. Keynes (1920). Volumen und hydratationswarme der ionen. *Physik A 1*, 45–48.

Hodgkin, A. and R. Keynes (1955). Active transport of cations in giant axons from Sepia and Loligo. *The Journal of Physiology 128*(1), 28.

Hoeflich, K. and M. Ikura (2002). Calmodulin in Action:: Diversity in Target Recognition and Activation Mechanisms. *Cell 108*(6), 739–742.

Hougaard, C., M. Jensen, R. Hummel, T. Johansen, B. Eriksen, D. Strøbæk, and P. Christophersen (2008). Positive modulation by the SK2/SK3-selective compound, CyPPA, is mediated via the C-terminal tail. *Biophys J 94*, 2199.

Ishii, T. M., C. Silvia, B. Hirschberg, C. T. Bond, J. P. Adelman, and J. Maylie (1997). A human intermediate conductance calcium-activated potassium channel. *Proceedings of the National Academy of Sciences of the United States of America 94*(21), 11651–11656.

Jones, H., M. Bailey, C. Baty, G. MacGregor, C. Syme, K. Hamilton, and D. Devor (2007). An NH2-terminal multi-basic RKR motif is required for the ATP-dependent regulation of hIK1. *Channels (Austin, Tex.) 1*(2), 80.

Jones, H., K. Hamilton, G. Papworth, C. Syme, S. Watkins, N. Bradbury, and D. Devor (2004). Role of the NH2 terminus in the assembly and trafficking of the in-

termediate conductance Ca2+-activated K+ channel hIK1. *Journal of Biological Chemistry 279*(15), 15531.

Kabsch W, S. C. (1983). Dictionary of protein secondary structure: pattern recognition of hydrogen-bonded and geometrical features. *Biopolymers 22 (12)*, 2577–2637.

Kaushal, V., P. Koeberle, Y. Wang, and L. Schlichter (2007). The Ca2+-activated K+ channel KCNN4/KCa3. 1 contributes to microglia activation and nitric oxide-dependent neurodegeneration. *Journal of Neuroscience 27*(1), 234.

Keen, J., R. Khawaled, D. Farrens, T. Neelands, A. Rivard, C. Bond, B. Janowsky, A. Fakler, J. Adelman, and J. Maylie (1999). Domains responsible for constitutive and ca(2+)-dependent interactions between calmodulin and small conductance ca(2+)-activated potassium channels. *The Journal of Neuroscience 19*, 8830–8838.

Kincaid, R., M. Nightingale, and B. Martin (1988). Characterization of a cDNA clone encoding the calmodulin-binding domain of mouse brain calcineurin. *Proceedings of the National Academy of Sciences of the United States of America 85*(23), 8983.

Klein, H., L. Garneau, U. Banderali, M. Simoes, L. Parent, and R. Sauve (2007). Structural determinants of the closed KCa3. 1 channel pore in relation to channel gating: results from a substituted cysteine accessibility analysis. *Journal of General Physiology 129*(4), 299.

Klein, H., L. Garneau, N. Trinh, A. Prive, F. Dionne, E. Goupil, D. Thuringer, L. Parent, E. Brochiero, and R. Sauve (2009). Inhibition of the KCa3. 1 channels by AMP-activated protein kinase in human airway epithelial cells. *American Journal of Physiology- Cell Physiology 296*(2), C285.

Kohler, M., B. Hirschberg, C. Bond, J. Kinzie, N. Marrion, J. Maylie, and J. Adelman (1996). Small-conductance, calcium-activated potassium channels from mammalian brain. *Science 273*(5282), 1709.

Latorre, R., C. Vergara, O. Alvarez, E. Stefani, and L. Toro (2000). *Voltage-gated calcium-modulated potassium channels of large unitary conductance: structure, diversity, and pharmacology*. Springer Verlag.

Lee, W., T. Ngo-Anh, A. Bruening-Wright, J. Maylie, and J. Adelman (2003). Small Conductance Ca2+-activated K+ Channels and Calmodulin. *Journal of Biological Chemistry 278*(28), 25940.

Li, W., D. Halling, A. Hall, and R. Aldrich (2009). EF hands at the N-lobe of calmodulin are required for both SK channel gating and stable SK–calmodulin interaction. *The Journal of general physiology 134*(4), 281.

Liu, M., T. Chen, B. Ahamed, J. Li, and K. Yau (1994). Calcium-calmodulin modulation of the olfactory cyclic nucleotide-gated cation channel. *Science 266*(5189), 1348.

Liu, M., B. Yu, O. Nakanishi, T. Wieland, and M. Simon (1997). The Ca2+-dependent Binding of Calmodulin to an N-terminal Motif of the Heterotrimeric G Protein β Subunit. *Journal of Biological Chemistry 272*(30), 18801.

Neher, E. and B. Sakmann (1976). Noise analysis of drug induced voltage clamp currents in denervated frog muscle fibres. *The Journal of Physiology 258*(3), 705.

O'Neil, K. and W. DeGrado (1990). How calmodulin binds its targets: sequence independent recognition of amphiphilic [alpha]-helices. *Trends in biochemical sciences 15*(2), 59–64.

Pedarzani, P., J. Mosbacher, A. Rivard, L. Cingolani, D. Oliver, M. Stocker, J. Adelman, and B. Fakler (2001). Control of electrical activity in central neurons by modulating the gating of small conductance Ca2+-activated K+ channels. *Journal of Biological Chemistry 276*(13), 9762.

Pedarzani, P. and M. Stocker (2008). Molecular and cellular basis of small- and intermediate-conductance, calcium-activated potassium channel function in the brain. *Cellular and Molecular Life Sciences 65*, 3196–3217.

Qin, F. (2004). Restoration of single-channel currents using the segmental k-means method based on hidden Markov modeling. *Biophysical journal 86*(3), 1488–1501.

Rettig, J., S. Heinemann, F. Wunder, C. Lorra, D. Parcej, J. Dolly, and O. Pongs (1994). Inactivation properties of voltage-gated K+ channels altered by presence of β-subunit.

Roux, B. and R. Sauve (1985). A general solution to the time interval omission problem applied to single channel analysis. *Biophysical journal 48*(1), 149–158.

Sali, A. and T. Blundell (1993). Comparative protein modelling by satisfaction of spatial restraints. *Journal Molecular Biology 234*, 779–815.

Sali, A., R. Sanchez, and A. Badretdinov (2001). MODELLER: A Program for Protein Structure Modeling Release 6. *Rockefeller University*.

Sankaranarayanan, A., G. Raman, C. Busch, T. Schultz, P. Zimin, J. Hoyer, R. Koehler, and H. Wulff (2008). SKA-31, a new activator of KCa2 and KCa3. 1 potassium channels, potentiates the EDHF response and lowers blood pressure. *Molecular Pharmacology*.

Schumacher, M., M. Crum, and M. Miller (2004). Crystal structures of apoc-

almodulin and an apocalmodulin/SK potassium channel gating domain complex. *Structure 12*(5), 849–860.

Schumacher, M., A. Rivard, H. Bachinger, and J. Adelman (2001). Structure of the gating domain of a Ca2+-activated K+ channel complexed with Ca2+/calmodulin. *Nature 410*(6832), 1120–1123.

Sheng, J., S. Ella, M. Davis, M. Hill, and A. Braun (2009). Openers of SKCa and IKCa channels enhance agonist-evoked endothelial nitric oxide synthesis and arteriolar vasodilation. *The FASEB Journal 23*(4), 1138.

Si, H., W. Heyken, S. Wolfle, M. Tysiac, R. Schubert, I. Grgic, L. Vilianovich, G. Giebing, T. Maier, V. Gross, et al. (2006). Impaired endothelium-derived hyperpolarizing factor-mediated dilations and increased blood pressure in mice deficient of the intermediate-conductance Ca2+-activated K+ channel. *Circulation research 99*(5), 537.

Simoes, M., L. Garneau, H. Klein, U. Banderali, F. Hobeila, B. Roux, L. Parent, and R. Sauve (2002). Cysteine mutagenesis and computer modeling of the S6 region of an intermediate conductance IKCa channel. *Journal of General Physiology 120*(1), 99.

Srivastava, S., L. Di, O. Zhdanova, Z. Li, S. Vardhana, Q. Wan, Y. Yan, R. Varma, J. Backer, H. Wulff, et al. (2009). The Class II Phosphatidylinositol 3 kinase C2 {beta} Is Required for the Activation of the K+ Channel KCa3. 1 and CD4 T-Cells. *Molecular Biology of the Cell 20*(17), 3783.

Srivastava, S., K. Ko, P. Choudhury, Z. Li, A. Johnson, V. Nadkarni, D. Unutmaz, W. Coetzee, and E. Skolnik (2006). Phosphatidylinositol-3 phosphatase myotubularin-related protein 6 negatively regulates CD4 T cells. *Molecular and cellular biology 26*(15), 5595.

Srivastava, S., Z. Li, K. Ko, P. Choudhury, M. Albaqumi, A. Johnson, Y. Yan, J. Backer, D. Unutmaz, W. Coetzee, et al. (2006). Histidine phosphorylation of the potassium channel KCa3. 1 by nucleoside diphosphate kinase B is required for activation of KCa3. 1 and CD4 T cells. *Molecular cell 24*(5), 665–675.

Stocker, J., L. De Franceschi, G. McNaughton-Smith, R. Corrocher, Y. Beuzard, and C. Brugnara (2003). ICA-17043, a novel Gardos channel blocker, prevents sickled red blood cell dehydration in vitro and in vivo in SAD mice. *Blood 101*(6), 2412.

Syme, C., K. Hamilton, H. Jones, A. Gerlach, L. Giltinan, G. Papworth, S. Watkins, N. Bradbury, and D. Devor (2003). Trafficking of the Ca2+-activated K+ channel, hIK1, is dependent upon a C-terminal leucine zipper. *Journal of Biological Chemistry 278*(10), 8476.

Toyama, K., H. Wulff, K. Chandy, P. Azam, G. Raman, T. Saito, Y. Fujiwara, D. Mattson, S. Das, J. Melvin, et al. (2008). The intermediate-conductance calcium-activated potassium channel KCa3. 1 contributes to atherogenesis in mice and humans. *The Journal of clinical investigation 118*(9), 3025.

Venema, R., H. Sayegh, J. Kent, and D. Harrison (1996). Identification, characterization, and comparison of the calmodulin-binding domains of the endothelial and inducible nitric oxide synthases. *Journal of Biological Chemistry 271*(11), 6435.

Vigil, D., S. Gallagher, J. Trewhella, and A. Garcia (2001). Functional dynamics of the hydrophobic cleft in the N domain of calmodulin. *Biophysical Journal 80*(5), 2082 – 2092.

Walker, S., K. Dora, N. Ings, G. Crane, and C. Garland (2001). Activation of endothelial cell IKCa with 1-ethyl-2-benzimidazolinone evokes smooth muscle hyperpolarization in rat isolated mesenteric artery. *British journal of pharmacology 134*(7), 1548–1554.

Wallace, A., R. Laskowski, and J. Thornton (1995). LIGPLOT: a program to generate schematic diagrams of protein-ligand interactions. *Protein Engineering Design and Selection 8*(2), 127.

Weiss, T. (1996). *Cellular biophysics*. Cambridge, Mass.

Wissmann, R., W. Bildl, H. Neumann, A. Rivard, N. Klocker, D. Weitz, U. Schulte, J. Adelman, D. Bentrop, and B. Fakler (2002). A helical region in the C terminus of small-conductance Ca2+-activated K+ channels controls assembly with apocalmodulin. *Journal of Biological Chemistry 277*(6), 4558.

Wulff, H., H. Knaus, M. Pennington, and K. Chandy (2004). K+ channel expression during B cell differentiation: implications for immunomodulation and autoimmunity. *The Journal of Immunology 173*(2), 776.

Wulff, H., A. Kolski-Andreaco, A. Sankaranarayanan, J. Sabatier, and V. Shakkottai (2007). Modulators of small-and intermediate-conductance calcium-activated potassium channels and their therapeutic indications. *Current medicinal chemistry 14*(13), 1437–1457.

Xia, X., B. Fakler, A. Rivard, G. Wayman, T. Johnson-Pais, J. Keen, T. Ishii, B. Hirschberg, C. Bond, S. Lutsenko, et al. (1997). Mechanism of calcium gating insmall-conductancecalcium-activated potassium channels. *Nature 386*, 167–170.

Yamamoto, Y., K. Imaeda, and H. Suzuki (1999). Endothelium-dependent hyperpolarization and intercellular electrical coupling in guinea-pig mesenteric arterioles. *The Journal of Physiology 514*(2), 505.

Yap, K., J. Kim, K. Truong, M. Sherman, T. Yuan, and M. Ikura (2000). Calmodulin target database. *Journal of structural and functional genomics 1*(1), 8–14.

Yap, K., T. Yuan, T. Mal, H. Vogel, and M. Ikura (2003). Structural basis for simultaneous binding of two carboxy-terminal peptides of plant glutamate decarboxylase to calmodulin. *Journal of molecular biology 328*(1), 193–204.

Yellen, G. (2001). Dimers among friends ion channel regulation by dimerization of tail domains. *Trends in pharmacological sciences 22*(9), 439–441.